Cyclin-dependent kinases regulate splice-specific targeting of dynamin-related protein 1 to microtubules

Stefan Strack, Theodore J. Wilson, and J. Thomas Cribbs

Department of Pharmacology, University of Iowa, Iowa City, IA 52246

Fission and fusion reactions determine mitochondrial morphology and function. Dynamin-related protein 1 (Drp1) is a guanosine triphosphate–hydrolyzing mechanoenzyme important for mitochondrial fission and programmed cell death. Drp1 is subject to alternative splicing of three exons with previously unknown functional significance. Here, we report that splice variants including the third but excluding the second alternative exon (x01) localized to and copurified with microtubule bundles as dynamic polymers that resemble fission complexes on mitochondria. A major isoform in immune cells, Drp1-x01 required oligomeric assembly and Arg residues in alternative exon 3 for microtubule targeting. Drp1-x01 stabilized and bundled microtubules and attenuated staurosporine-induced mitochondrial fragmentation and apoptosis. Phosphorylation of a conserved Ser residue adjacent to the microtubule-binding exon released Drp1-x01 from microtubules and promoted mitochondrial fragmentation in a splice form–specific manner. Phosphorylation by Cdk1 contributed to dissociation of Drp1-x01 from mitotic microtubules, whereas Cdk5-mediated phosphorylation modulated Drp1-x01 targeting to interphase microtubules. Thus, alternative splicing generates a latent, cytoskeletal pool of Drp1 that is selectively mobilized by cyclin-dependent kinase signaling.

Introduction

The diverse functions of mitochondria in bioenergetics, secondary metabolism, calcium homeostasis, and apoptosis are inextricably linked to the shape of the organelle, which can range from spherical to highly interconnected within the same cell. A group of large GTPases of the dynamin family are responsible for mitochondrial shape changes and essential for organismal viability (Chen et al., 2003; Davies et al., 2007; Waterham et al., 2007; Ishihara et al., 2009; Wakabayashi et al., 2009). Mitochondrial fusion is performed by three transmembrane GTPases: outer membrane fusion by mitofusin-1 and -2 and inner membrane fusion by Opa1 (optic atrophy 1). Mitochondrial division (fission) is catalyzed by a single GTPase, namely dynamin-related protein 1 (Drp1) or dynamin-like protein 1 (gene DNM1L; Hoppins et al., 2007). Drp1 also mediates fission of peroxisomes (Koch et al., 2003; Ishihara et al., 2009; Wakabayashi et al., 2009). Drp1 cycles between cytosol and mitochondria, where it forms spiral-shaped superstructures that hydrolyze GTP to constrict and ultimately sever mitochondria, likely involving conformational rearrangements similar to dynamin pinching off endocytic vesicles (Morlot and Roux, 2013). Whereas the dynamins bind membranes via a pleckstrin homology domain, Drp1 is recruited to mitochondria by dedicated outer mitochondrial membrane (OMM)–anchored receptor proteins (Otera et al., 2013). Drp1 consists of an N-terminal GTPase, followed by middle, variable, and C-terminal GTPase effector domains (Fig. 1 A). Positioned like the pleckstrin homology domain in dynamin, the variable domain of Drp1 is dispensable for mitochondrial localization and activity of the fission enzyme (Strack and Cribbs, 2012).

Drp1 is subject to regulation at multiple levels, including transcription, proteasomal degradation, sumoylation, S-nitrosylation, O-glycosylation, and reversible phosphorylation (Otera et al., 2013; Wilson et al., 2013). It has long been recognized that Drp1 is diversified by alternative splicing of the GTPase and variable domain; however, functional consequences remained unknown

Correspondence to Stefan Strack: stefan-strack@uiowa.edu

Abbreviations used in this paper: ANOVA, analysis of variance; Drp1, dynamin-related protein 1; KO, knockout; MEF, mouse embryonic fibroblast; MT, microtubule; OMM, outer mitochondrial membrane; PBMC, primary blood monocyte cell; qRT-PCR, quantitative real-time PCR.

The Rockefeller University Press $30.00
J. Cell Biol. Vol. 201 No. 7 1037–1051
www.jcb.org/cgi/doi/10.1083/jcb.201210045

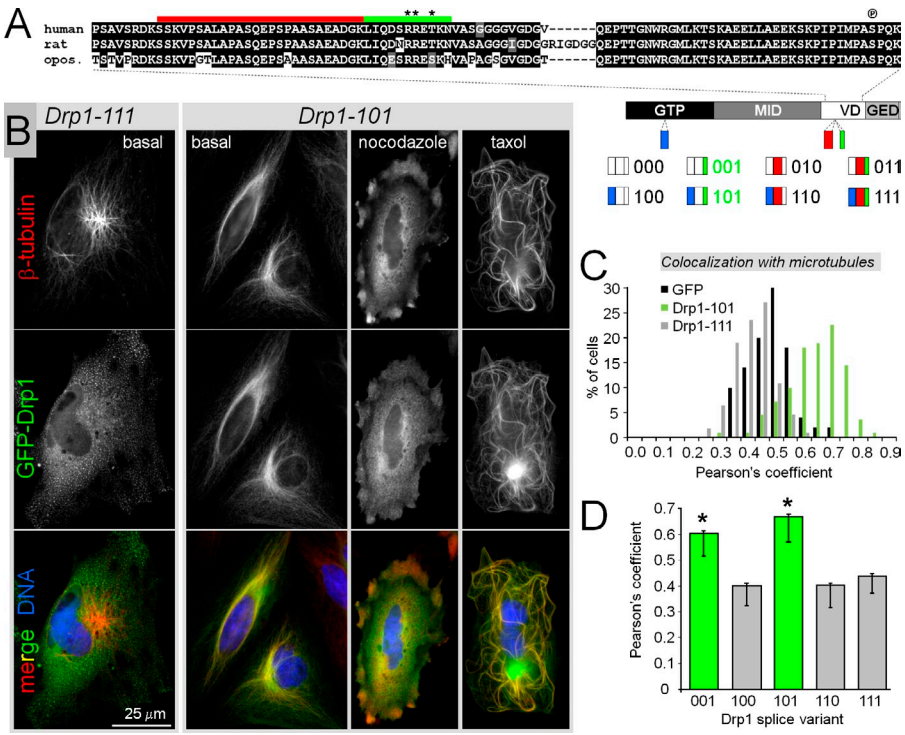

Figure 1. **Drp1-001 and -101 splice variants localize to the interphase MT cytoskeleton.** (A) Shown is a domain diagram of Drp1 with an alignment of the central portion of the variable domain (VD) containing the second (red) and third (green) alternative exon from human, rat, and opossum (opos.). Black star and encircled "P" indicate critical residues and the Ser_{CDK} phosphorylation site, respectively. (B–D) HeLa cells expressing the indicated GFP-tagged Drp1 splice variants in place of endogenous Drp1 were analyzed for colocalization of the mitochondrial fission enzyme with β-tubulin by immunofluorescence. (B) Representative epifluorescence images of cells under basal conditions, after MT depolymerization (100 ng/ml nocodazole, 6 h), and after MT stabilization (10 µM taxol, 6 h) show that Drp1-101 follows the distribution of β-tubulin in different polymerization states. Drp1 colocalization with β-tubulin was quantified as the Pearson's coefficient and is shown as a frequency distribution (C) and population means (D; means ± SEM [up]/SD [down] of ∼100 cells). *, $P < 10^{-15}$ compared with all cytosolic splice variants.

(Yoon et al., 1998; Howng et al., 2004; Uo et al., 2009). Here, we report that alternative splicing controls the subcellular localization of Drp1 and provide a mechanism by which cyclin-dependent kinases promote mitochondrial fission in a Drp1 isoform–specific manner.

Results

Select Drp1 splice variants localize to microtubules (MTs)

Mammalian Drp1 genes include three alternative exons, one encoding an insert between subdomains A and B of the GTPase domain and two encoding consecutive regions of the variable domain (Fig. 1 A). Alternative exons are short (11–26 codons), but well conserved (Fig. 1 A), suggesting functional importance. Independent inclusion of the three exons gives rise to 2^3 = 8 coding variants of Drp1, all of which are represented in expressed sequence tag databases. Because there is little consensus in splice variant numbering between species, we adopted a three-digit binary nomenclature, in which 0 indicates absence and 1 presence of an alternative exon at positions 1, 2, and 3. The shortest Drp1 variant is hence referred to as 000 and the longest as 111 (Fig. 1 A).

To characterize individual Drpl splice variants in cells, we expressed them as GFP fusion proteins from plasmids that also express an shRNA to silence endogenous Drp1 (Cribbs and Strack, 2007). Replacing endogenous Drp1 isoforms with specific splice variants in HeLa cells, we found that six of the eight splice variants (000, 010, 011, 100, 110, and 111) exhibited a largely diffuse, cytosolic distribution with some puncta as noted before (Pitts et al., 1999; Frank et al., 2001). In striking contrast, the two Drp1 isoforms that lack the second but include the third alternative exon (001 and 101 = x01) colocalized extensively with the MT network in interphase HeLa cells (Fig. 1 B). The filamentous localization of GFP-Drp1-x01 was abolished by depolymerizing MTs with nocodazole, whereas the MT-stabilizing drug taxol bundled both MTs and GFP-Drp1-x01 into convoluted, cable-like structures (Fig. 1 B). Colocalization of GFP-Drp1-001 and -101 with β-tubulin was confirmed by quantitative image analysis (Merrill et al., 2011), with other Drp1 splice variants achieving Pearson's coefficients similar to GFP alone (Fig. 1, C and D). Similar immunofluorescence experiments with COS, PC12, Jurkat, primary astroglial cells, and Drp1 knockout (KO) mouse embryonic fibroblasts (MEFs) established that splice form–specific localization of Drp1 is cell type independent (Fig. S1 A and not depicted). In addition, Drp1 variants without epitope tags (visualized via Drp1 immunofluorescence) localized indistinguishably from their GFP-tagged counterparts (unpublished data).

Expression profile of Drp1 splice and phosphorylation variants

We next profiled Drp1 splice form expression in cell lines and tissues. Quantitative real-time PCR (qRT-PCR) with primer sets bridging alternative splice sites was used to quantify inclusion of N- and C-terminal alternative exons separately (Fig. S1 D). Drp1 mRNA lacking the alternative insert in the GTPase domain (0xx) outnumbered mRNA containing this insert (1xx) in six primary cells and cell lines examined (Fig. S1 E). Except for primary rat astroglia, in which Drp1-000 constituted ∼90% of total Drp1 mRNA, Drp1-001 was a major isoform, predominating over other splice variants in human primary blood monocyte cells (PBMCs; containing mostly activated T lymphocytes) and Jurkat cells, a line derived from human T cells (∼80% of total). Human HeLa, simian COS1, and rat PC12 cells contained 40–60% 001 mRNA, with 000 comprising most of the remainder (Fig. S1 E).

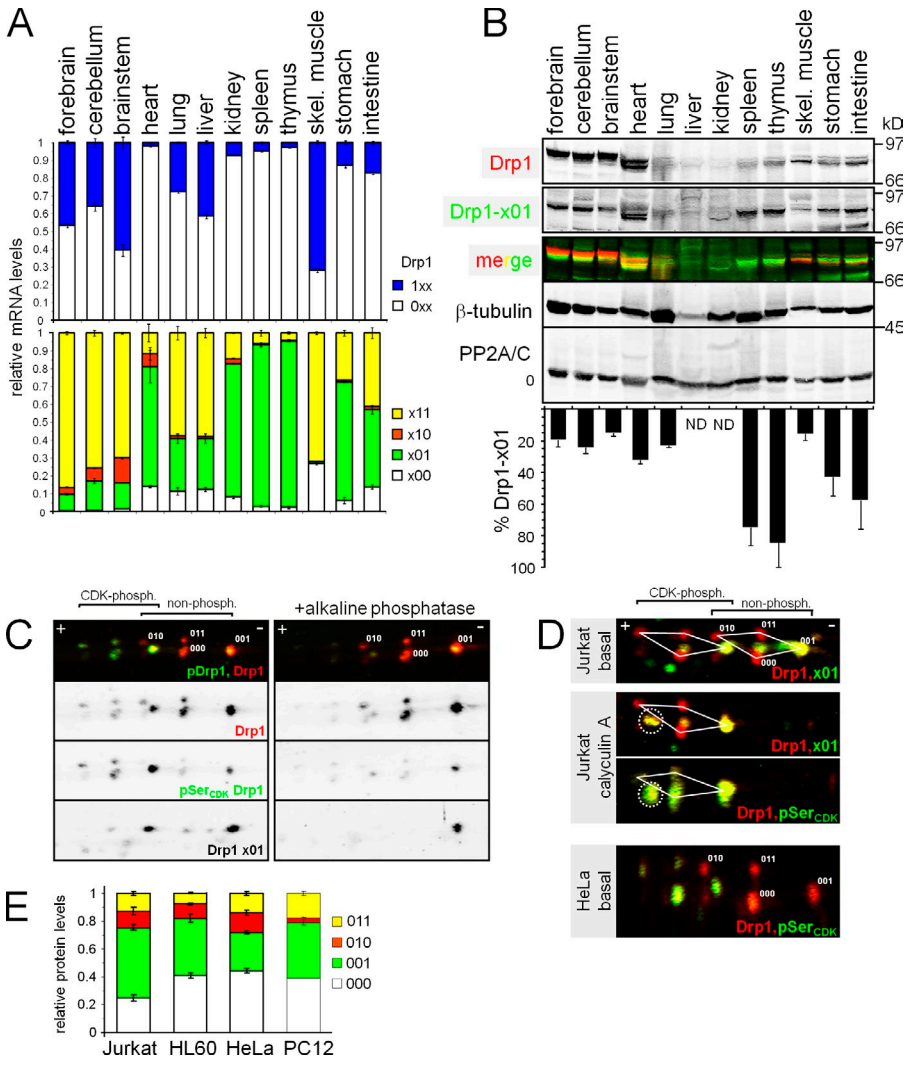

Figure 2. **MT-targeted Drp1 is a major isoform at mRNA and protein levels.** (A) RNA from the indicated mouse tissues was analyzed by qRT-PCR with Drp1 splice-specific primer sets (means ± SEM, *n* = 3). (B) Triton X-100 extracts of the indicated mouse tissues (15–30 µg/lane) were subjected to immunoblotting for the indicated proteins, and relative expression of Drp1-x01 was quantified as the ratio of x01 to pan-Drp1 antibody signals standardized by signals in an adjacent lane with extract containing GFP-Drp1-001 (100%; means ± SEM, *n* = 3). (C–E) Quantification of Drp1 isoform expression and phosphorylation by 2D immunoblotting is shown. (C) Total PC12 lysates were treated with or without alkaline phosphatase and separated by 2D PAGE. One set of blots was coincubated with antibodies to total and Ser_{CDK}-phosphorylated Drp1, whereas a second set was probed for Drp1-x01. (D) Similar 2D immunoblotting experiments identify Drp1 splice and phosphorylation variants in Jurkat and HeLa cells. Trapezoids highlight the major Drp1 splice variant constellation ± Ser_{CDK} phosphorylation; dashed circles indicate a hyperphosphorylated form of Drp1-001 generated by PP1/PP2A inhibition via calyculin A (25 nM, 1 h). (E) Relative Drp1 splice variant protein expression was quantified by densitometry of 2D blots probed for total Drp1 (means ± SEM, *n* = 3).

In the adult mouse, Drp1 with the GTPase insert (1xx) was highly expressed (>30%) in brain (forebrain, brainstem, and cerebellum), skeletal muscle, and liver (Fig. 2 A). The two most abundant Drp1 variable domain variants in mouse tissues were x11 and x01. Drp1-x11 predominated in the three brain regions examined, lung, liver, and skeletal muscle, whereas x01 was the most abundant isoform in heart, kidney, spleen, thymus, stomach, and intestine (Fig. 2 A). Spleen and thymus contained the highest proportion of the x01 variant (~90%), which together with high expression in human PBMCs and Jurkat T cells suggests that Drp1-x01 has a specialized role in immune cells. Similar Drp1 splice patterns were detected in a subset of rat tissues examined (brain, heart, and liver; unpublished data).

To confirm these results at the protein level, we immunized rabbits with an 11–amino acid peptide that bridges the N terminus of the third alternative exon and adjacent common amino acids (Fig. S1 F). Antibodies recognized ectopically expressed x01, but not other isoforms, including x11, which contains the entire immunogenic sequence, albeit divided by insertion of the second alternative exon (Fig. S1 G). The Drp1-x01–specific antibody reacted with Drp1 immunoprecipitated from COS1 cells, which express high levels of 001 mRNA, but not from primary astroglia, which do not (Fig. S1 H). We used the x01-specific and a pan-Drp1 antibody to quantify relative Drp1-x01 protein abundance in Triton X-100 extracts of the same 12 mouse tissues subjected to Drp1 mRNA profiling above. Extracts from HeLa cells expressing GFP-Drp1-001 accounted for differences in detection efficiency by the two antibodies. With the exception of heart, in which high levels of x01 mRNA but moderate levels of x01 protein were detected, Drp1-x01 protein and mRNA tissue profiles were in good agreement, confirming that this splice variant predominates in spleen and thymus (Fig. 2 B). Because of low total Drp1 signals, Drp1-x01 protein proportions could not be accurately quantified in liver and kidney extracts (note, however, the x01-positive band in extracts from kidney, an organ with high x01 mRNA levels).

We next combined 2D electrophoresis with dual-channel immunoblotting to quantify protein levels of all Drp1 splice variants. The two C-terminal alternative inserts are differentially charged (Drp1-001, pI = 6.48; Drp1-010, pI = 6.27), allowing for separation of similar mass Drp1 isoforms by isoelectric focusing on narrow pH gradients. 2D Western blotting of Jurkat cell extracts with the pan-Drp1 antibody detected eight to ten Drp1 spots, rather than the three to four spots anticipated from mRNA profiling. According to predicted molecular mass and pI, as well as recognition by the splice-specific antibody, two of

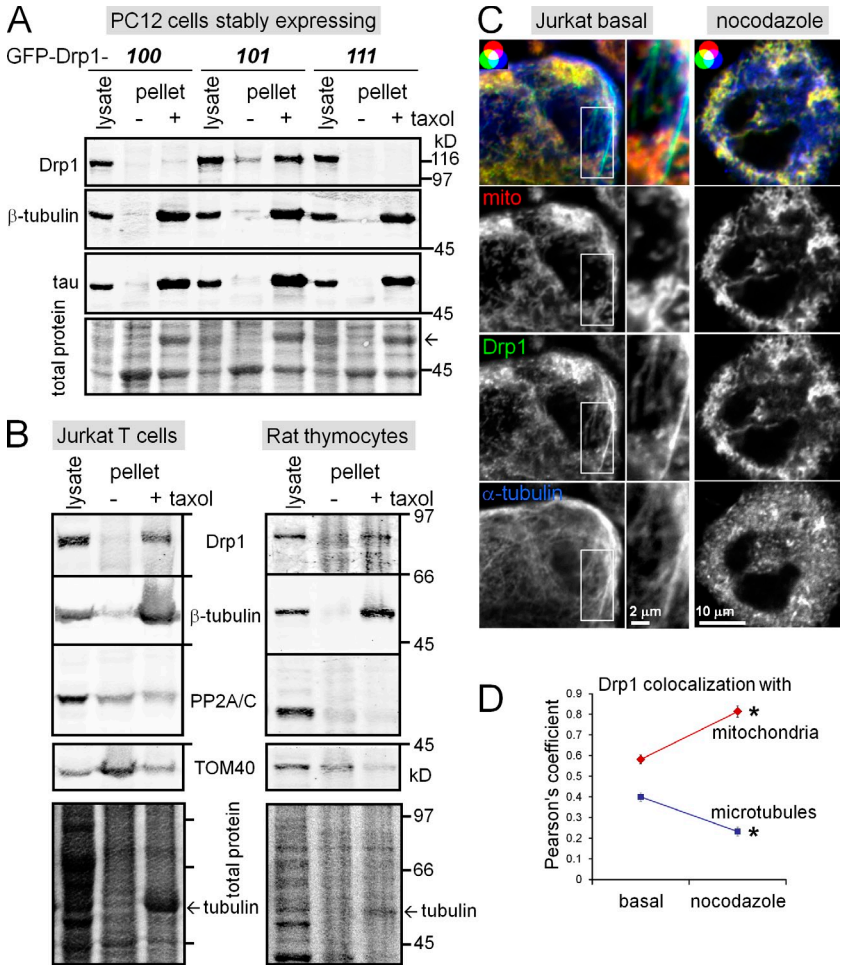

Figure 3. **Endogenous Drp1-x01 copurifies and colocalizes with MTs.** (A) PC12 cells stably expressing GFP-tagged Drp1-100, -101, and -111 were lysed ± taxol (10 µM) and lysates were subjected to centrifugation through a 1-M sucrose cushion. (B) Similar experiments with Jurkat cells and acutely dissociated rat thymocytes show copurification of endogenous Drp1 with MTs. About 5% of the lysate and 10% of the pellets was loaded. Total protein was visualized by staining blots with Ponceau S before antibody incubation. (C and D) Jurkat cells treated ± nocodazole (100 ng/ml, 2 h) were immunolabeled for mitochondria (TOM20), Drp1, and α-tubulin and imaged by confocal microscopy (C; representative images). MT depolymerization decreases colocalization of endogenous Drp1 with α-tubulin, but increases colocalization with mitochondria (D; means ± SEM of 49 and 23 cells). *, $P < 10^{-6}$.

these spots derived from the 001 variant. A group of four to five spots toward the acidic end of the pH gradient (one of which identified as 001) was also immunoreactive for Drp1 phosphorylated at a CDK1/cyclin B site (Taguchi et al., 2007), and these spots disappeared when cell extracts were incubated with alkaline phosphatase before isoelectric focusing (Fig. 2 C). Conversely, treating Jurkat cells with the PP1/PP2A inhibitor calyculin A before lysis (25 nM, 1 h) resulted in a quantitative leftward (acidic) shift of the Drp1 spot constellation and identical staining patterns with phospho- and total Drp1 antibodies, indicative of fully stoichiometric phosphorylation at Ser_{CDK} (Fig. 2 D). Phosphatase inhibition also generated a new, acidic isoelectric point variant (circled in Fig. 2 D), likely representing Drp1-001 dually phosphorylated on Ser_{CDK} and a second site, perhaps Ser_{PKA} (Chang and Blackstone, 2007; Cribbs and Strack, 2007; Cereghetti et al., 2008). Densitometry of phosphorylated versus nonphosphorylated Drp1 isoelectric point variants in unsynchronized HeLa and Jurkat cell populations demonstrated that 35–40% of Drp1 is phosphorylated at Ser_{CDK}, regardless of splice variant. Largely mirroring mRNA levels (Fig. S1 E), 2D Western blotting and densitometry also indicated that 001 is the most abundant Drp1 isoform in Jurkat cells and 000 and 001 splice forms are present at similar levels in human leukocytic HL60 and PC12 cells, whereas HeLa cells contain more 000 than 001 (Fig. 2, D and E). Thus, MT-targeted Drp1-001 is abundantly expressed in many cell lines and tissues analyzed, constituting the large majority of Drp1 in tissues and cells of the immune system.

Endogenous Drp1-x01 copurifies and colocalizes with MTs

To provide biochemical evidence for MT association of Drp1-x01, we generated PC12 cell lines that stably express GFP-Drp1-110, 101, or 111 to similar levels. Triton X-100–containing cell lysates were prepared with and without taxol and subjected to centrifugation. Taxol sedimented not only MTs and the MT-associated protein tau, but also Drp1-101, whereas the other two Drp1 splice variants remained in the supernatant (Fig. 3 A). Similarly, endogenous Drp1 robustly copurified with MTs from Jurkat T cells (Fig. 3 B) in which Drp1-001 contributes the majority of the total Drp1 pool (Fig. 2 E). We also isolated MTs from acutely dissociated rat thymus, the origin of mature T cells. In agreement with Drp1 mRNA and protein profiling in mouse thymus (Fig. 2, A and B), rat thymocyte Drp1 migrated as a single band and was recovered in the MT pellet (Fig. 3 B). TOM40, a protein of the OMM, was depleted from the taxol-stabilized pellet, ruling out a role for mitochondria in Drp1 sedimentation in these assays.

To confirm colocalization of endogenous Drp1 with MTs, Jurkat cells were immunofluorescently labeled for pan-Drp1, α-tubulin, and mitochondria (TOM20) and imaged by confocal

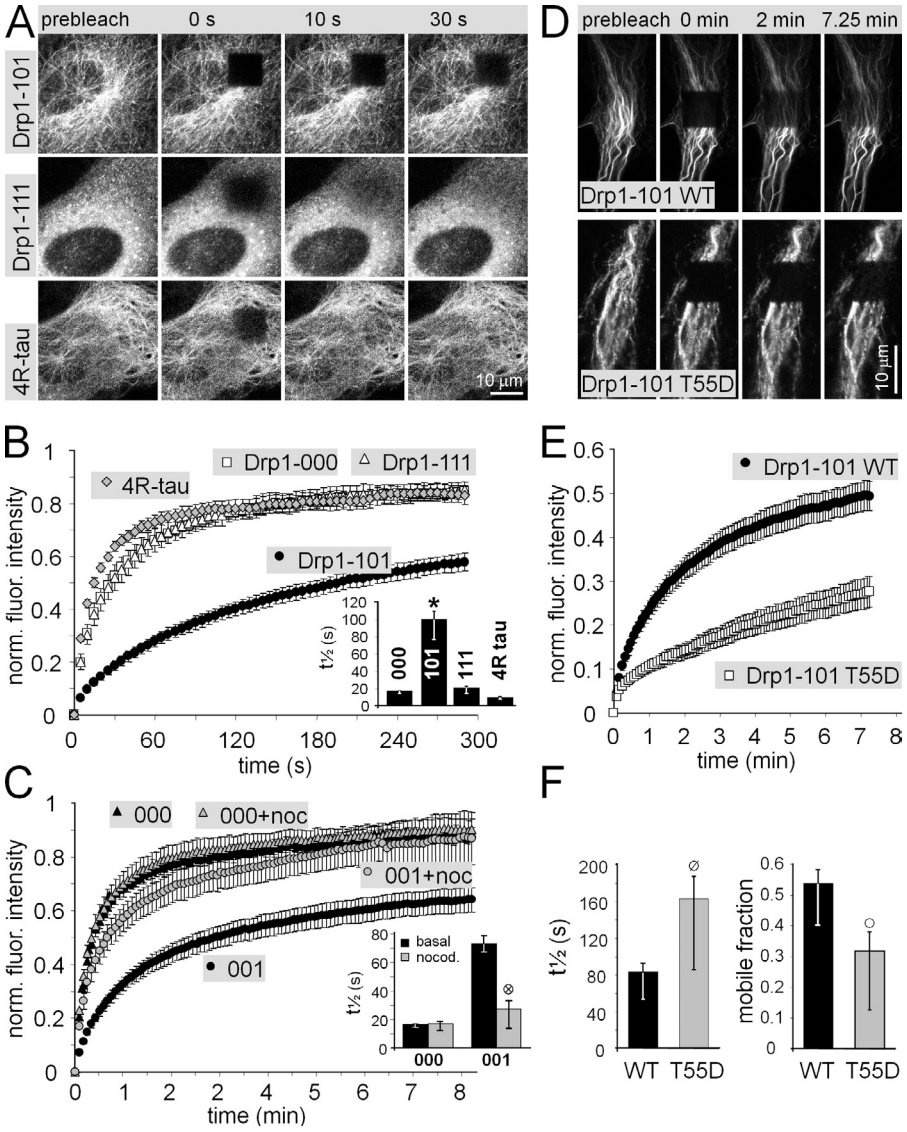

Figure 4. **Fluorescence recovery of Drp1 is modulated by MT association and GTP hydrolysis.** (A–F) A square in the cytosol of HeLa cells expressing the indicated GFP-tagged proteins was bleached and fluorescence recovery was monitored every 5 s for up to 8 min. Frames of representative time series are shown in A and D, whereas recovery curves and kinetic parameters derived from biexponential fits of the recovery curves (50% recovery time, $t_{1/2}$; mobile fraction) are plotted in B, C, E , and F (means ± SEM [up]/SD [down] of 6–8 cells). ○, $P < 0.05$; ∅, $P < 0.01$; ⊗, $P < 0.005$; *, $P < 0.0001$.

microscopy (Fig. 3 C). Endogenous Drp1 displayed a mixed distribution, decorating prominent MT bundles, but also mitochondria. MT depolymerization via nocodazole reduced colocalization of Drp1 with α-tubulin but increased colocalization with mitochondria as quantified by Pearson's coefficient (Fig. 3, C and D).

Heterooligomerization modulates Drp1 targeting to MTs

Endogenous Drp1 did not colocalize or copurify with MTs from HeLa cells (not depicted), a cell line with moderate levels of Drp1-001 (27%; Fig. 2 E), suggesting a threshold for MT association. Drp1 is an obligate tetramer, which assembles further into higher-order oligomers (Hoppins et al., 2007). It is therefore conceivable that MT binding of Drp1-x01 is modulated by heterooligomerization with other splice variants. To test whether Drp1 can form mixed oligomers, COS1 cells expressing permutations of four HA-tagged and six GFP-tagged splice variants were subjected to coimmunoprecipitation. In some experiments, cells were treated with a cell-permeant, reversible cross-linker before lysis to stabilize higher-order Drp1 structures. Under either condition, Drp1 formed homooligomers as efficiently as heterooligomers (Fig. S2 A and not depicted). These results indicate that the fission enzyme exists in cells as a homogenous pool of oligomers with a composition determined by relative splice form expression.

We next examined subcellular targeting of mixed Drp1 oligomers, replacing endogenous Drp1 in HeLa cells with varying ratios of MT-bound (101) and cytosolic (111) isoforms. Dose-dependent recruitment of Drp1 to MTs was observed, with cells expressing 100% and 75% of the 101 splice form showing robust colocalization of Drp1 with MTs (Fig. S2, B and C). With the caveat that a minor MT-localized Drp1 pool may be difficult to detect against a background of the cytosolic GTPase, these results suggest that Drp1 tetramers with three or more x01 subunits are efficiently recruited to MTs.

Slow exchange kinetics of Drp1-x01 depend on GTP hydrolysis

To investigate whether alternative splicing affects the mobility of Drp1, we quantified FRAP in HeLa cells in which endogenous Drp1 was replaced with individual, GFP-tagged splice variants.

The two cytosolic splice variants tested (000 and 111) displayed identical and rapid recovery kinetics (50% recovery time, $t_{1/2}$ = ~20 s; Fig. 4, A and B; and Video 1). In contrast, turnover of the two MT-bound isoforms (001 and 101) was markedly slower ($t_{1/2}$ = 75–100 s). Unexpectedly, tau, specifically the splice form with four MT-binding repeats (4R), cycled faster than even the cytosolic Drp1 splice forms ($t_{1/2}$ = 8–10 s), suggesting that the MT interaction per se may not be rate limiting for the slow exchange of Drp1-x01. To confirm that the slow mobility of Drp1–x01 depends on an intact cytoskeleton, we determined FRAP kinetics in the presence of nocodazole. MT depolymerization accelerated GFP-Drp1-001 recovery almost to the level of cytosolic Drp1, which in turn was insensitive to nocodazole (Fig. 4 C).

Why does Drp1-x01 cycle an order of magnitude more slowly between bound and unbound states than the classical MT-binding protein 4R-tau? We reasoned that Drp1-x01 association with MTs may involve GTPase-dependent assembly/disassembly cycles, which are slower than the on- and off-rate constants for MT binding. Indeed GTP hydrolysis is required for MT association of Drp1-x01 because GTPase-deficient Drp1 K38A localized to spherical cytosolic aggregates with no obvious relationship to mitochondria or MTs regardless of splice context (unpublished data). Next, we introduced the T55D mutation into Drp1's GTPase domain, which in the context of dynamin-2 was shown to moderately attenuate GTP hydrolysis (Song et al., 2004). In contrast to K38A, T55D did not perturb Drp1-101's MT localization. It did, however, significantly slow down fluorescence recovery as indicated by an increase in $t_{1/2}$ and a decrease in the mobile fraction (Fig. 4, D–F). These experiments indicate that GTP hydrolysis is the rate-limiting step in the exchange of cytoskeletal Drp1-x01 and suggest that mitochondria and MT targeting of the fission enzyme may be mechanistically similar.

Drp1-x01 stabilizes and bundles MTs

MT-associated proteins influence structure and dynamics of the MT cytoskeleton by diverse mechanisms, including modulation of tubulin polymerization/depolymerization rates, lateral assembly of MTs into bundles, and cross-bridging to other cellular structures (Walczak and Shaw, 2010; de Forges et al., 2012). To obtain initial evidence for effects of Drp1-x01 on MT dynamics, we monitored two posttranslational modification signatures on α-tubulin. C-terminal tyrosination of α-tubulin by tubulin tyrosine ligase is a marker of nascent and dynamic MTs, whereas acetylation of α-tubulin at Lys40 is predominantly associated with stable MTs (Hammond et al., 2008; Szyk et al., 2011). We colabeled HeLa expressing GFP-Drp1-111, GFP-Drp1-101, or GFP with monoclonal antibodies specific for the two modification states on α-tubulin and quantified MT stability as the ratio of acetylated to tyrosinated α-tubulin immunofluorescence intensity for each cell. Drp1-101 replacement significantly increased this ratio compared with Drp1-111 or vector (GFP) transfection (Fig. 5, A and B), indicating that Drp1-x01 promotes MT stability.

To investigate the consequence of Drp1-x01 expression for the structural organization of the MT cytoskeleton, a MT bundling index was calculated as the ratio of area to perimeter of the autosegmented, α-tubulin–immunolabeled MT network. As MTs form bundles, perimeter decreases with unchanged area, as was validated by brief taxol treatment (unpublished data). Drp1-101 expression promoted bundling of both tyrosinated (dynamic) and acetylated (stable) MTs (Fig. 5, C and D). Bundling of stable MTs was more pronounced, presumably because tyrosinated MT bundles represent a transition state in the conversion to acetylated MT bundles.

We next visualized MT dynamics directly, measuring FRAP of EYFP-tagged α-tubulin in HeLa cells also expressing mCherry-Drp1-111, mCherry-Drp1-101, or mCherry alone (Fig. 5, E–G). As a positive control, MT stabilization by taxol greatly attenuated α-tubulin fluorescence recovery (increase in time to 50% recovery from 8 to 68 s). Whereas Drp1-111 had no effect, MT-targeted Drp1-101 slowed α-tubulin dynamics significantly ($t_{1/2}$ = 16 s; Fig. 5, E–G). In combination, these results indicate that Drp1-x01 can confer increased stability to the MT cytoskeleton.

MT binding sequesters Drp1 from mitochondria, leading to mitochondrial elongation and slowing of apoptosis onset

How does alternative exon selection in the Drp1 premRNA influence mitochondrial morphology? We found that MT binding decreases colocalization of Drp1 with mitochondria (Fig. 6, A and B). This apparent sequestration of Drp1-x01 was accompanied by moderate but reproducible mitochondrial elongation (Fig. 6, A and C). Compared with untransfected HeLa cells that express a mixture of cytosolic and MT-targeted splice variants, isoform replacement with Drp1-x01 resulted in an increase in area-weighted form factor, a measure of shape complexity that accounts for object area (Merrill et al., 2011). Conversely, replacement with cytosolic Drp1 splice variants produced mitochondrial fragmentation. Splice form–specific changes in mitochondrial shape were observed in unperturbed cultures, as well as in cultures in which mitochondrial fragmentation was induced by a nitric oxide donor or by depolarizing mitochondria with a protonophore (Fig. 6 C). We also assessed the ability of Drp1 splice forms to restore mitochondrial fission in Drp1 KO MEFs. Transient transfection of either Drp1-111 or -101 resulted in a decrease in mitochondrial length; however, Drp1-111 expressing Drp1 KO MEFs had significantly shorter mitochondria than those expressing the MT-targeted isoform (Fig. S1, B and C).

Inhibition of mitochondrial fission raises the threshold for apoptosis induction (Kageyama et al., 2011; Youle and van der Bliek, 2012). To explore the role of Drp1 alternative splicing in apoptosis, endogenous Drp1 in primary rat astrocytes (predominantly the 000 isoform; Fig. S1 E) was exchanged with either Drp1-001 or -010 by transient transfection. Similar to HeLa cells, astrocytes expressing MT-targeted Drp1 had longer mitochondria than astrocytes expressing the cytosolic splice form. The broad spectrum kinase inhibitor staurosporine (1 µM) induced rapid (<1 h) mitochondrial fragmentation, which was attenuated by Drp1-001 expression (Fig. 6, D and E). The degree of attenuation is underestimated by the morphometric analysis, which frequently misidentifies as fragmented mitochondria the swollen but clearly interconnected mitochondrial particles seen in Drp1-001 expressing astrocytes treated for 2–3 h in staurosporine (Fig. 6 D). Whereas staurosporine promoted rapid translocation of Drp1-010 from the cytosol to mitochondria, Drp1-001 retained its cytoskeletal localization throughout the time course analyzed (Fig. 6 D, insets).

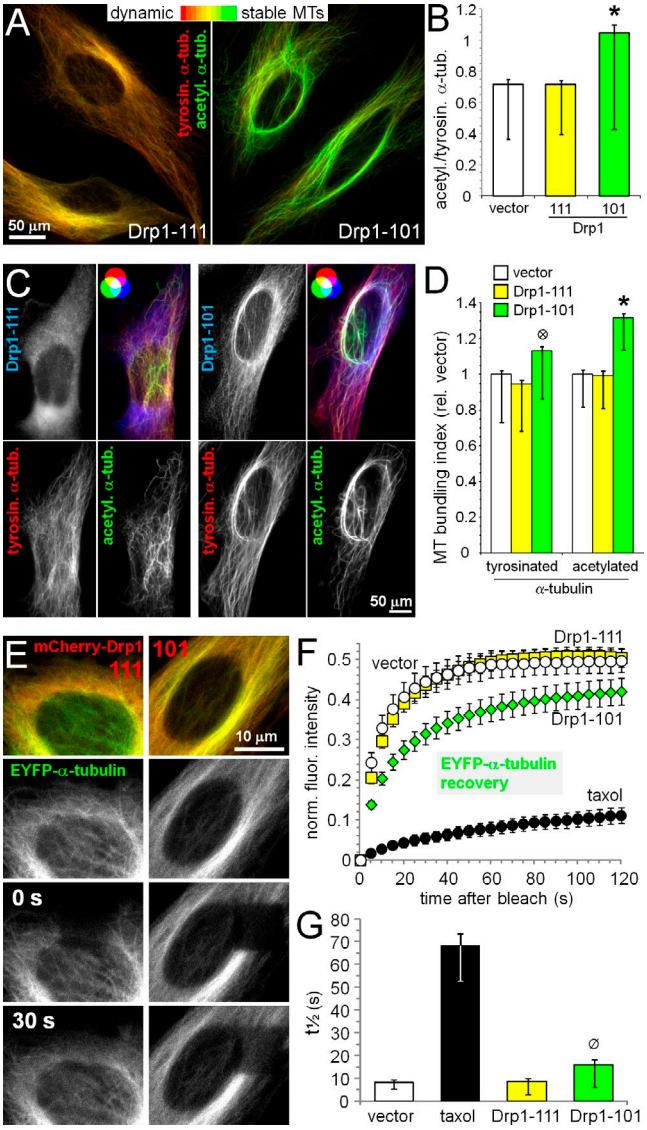

Figure 5. **Drp1-x01 promotes MT stability.** (A and B) HeLa cells expressing GFP (vector), GFP-Drp-111, or GFP-Drp–101 were immunofluorescently labeled for tyrosinated (tyrosin., dynamic, red) and acetylated (acetyl., stable, green) α-tubulin (α-tub.) and imaged by epifluorescence microscopy with constant camera settings. (A) Representative overlays of red and green channels. Drp1-101 increases MT stability quantified as the ratio of acetylated to tyrosinated α-tubulin signals integrated over the entire cell (B; means ± SEM [up]/SD [down] of 170–178 cells). (C and D) HeLa cells transfected, labeled, and imaged as in A and B were subjected to MT morphometry, quantifying MT bundling as an increase in the area/perimeter ratio of the autosegmented MT network. Representative epifluorescence images (C) and bar graph (D; means ± SEM [up]/SD [down] of 150–199 cells) show that Drp1-x01 induces bundling of MTs. (E–G) HeLa cells co-expressing EYFP-α-tubulin and mCherry-Drp1-111, mCherry-Drp1-101, or mCherry (vector) alone were analyzed for recovery of EYFP-α-tubulin after photobleaching; vector-transfected cells were also treated with taxol (10 µM, 3 h). Frames of representative time series are shown in E, whereas recovery curves and 50% recovery time ($t_{1/2}$) derived from biexponential fits of the recovery curves are plotted in F and G (means ± SEM [up]/SD [down] of 7–20 cells). ∅, $P < 0.01$; ⊗, $P < 10^{-6}$; *, $P < 10^{-9}$.

In addition to inhibiting mitochondrial fission, expression of Drp1-001 also delayed apoptosis onset in primary astroglia (~50% reduction in apoptotic nuclei 3 and 4 h after staurosporine addition; Fig. 6 F). To confirm these results, we compared sensitivity to staurosporine in Drp1 KO MEFs reconstituted with three Drp1 splice variants (Fig. 6, G and H). Compared with GFP, re-expression of Drp1 resulted in a pronounced increase in the number of apoptotic cells. However, MEFs expressing MT-targeted Drp1-001 were significantly less sensitive to staurosporine than MEFs expressing Drp1-000 or -011 (Fig. 6, G and H). Thus, similar to Drp1 knockdown or dominant-negative inhibition (Frank et al., 2001), the MT-binding exon interferes with Drp1 recruitment to mitochondrial fission foci to confer at least partial protection against apoptotic cell death.

Determinants for Drp1-x01 association with MTs

The results so far indicate that the 11–amino acid long, third alternative exon acts as a MT-binding domain unless the adjacent second alternative exon is also part of the Drp1 mRNA. To further investigate the structural and sequence requirements for MT association of Drp1, we performed site-directed mutagenesis (Fig. 7 A). Predicted to map to a loop that mediates oligomerization (Faelber et al., 2011; Ford et al., 2011), the G363D substitution allows Drp1 to dimerize, but prevents its assembly into tetramers and larger oligomers (Ingerman et al., 2005; Chang et al., 2010; Strack and Cribbs, 2012). When expressed in HeLa cells, GFP-Drp1-101 G363D displayed a cytosolic localization pattern devoid of discrete structures (Fig. 7 B), colocalized no better than cytosolic Drp1-100 with MTs (Fig. 7 C), and resulted in less mitochondrial elongation than wild-type Drp1-101 (Fig. 7 D). FRAP studies revealed that the oligomerization-impaired mutant is hypermotile, diffusing faster than even cytosolic Drp1 (Fig. 7, E and F). In combination with the mixed oligomer experiments (Fig. S2, B and C), these results indicate that MT association of Drp1 requires multivalent interactions between residues encoded by alternative exon 3 and the α/β-tubulin polymer. Although lacking a strict sequence consensus, MT-binding domains commonly contain positively charged residues thought to interact electrostatically with the acidic C termini of α- and β-tubulin (Downing, 2000). Indeed, when two adjacent arginine residues in the MT-binding exon were replaced with alanine (RR566AA mutant), Drp1-101 behaved indistinguishably from cytosolic Drp1-111 in terms of localization (Fig. 7, B and C), mitochondrial fission activity (Fig. 7 D), and mobility (Fig. 7, E and F). Apart from mediating the MT interaction of Drp1-x01, Arg566 and 567 also form part of a consensus motif for phosphorylation by the large family of Arg-directed protein kinases (RRX[S/T]; RRET in human and rodent and RRES in opossum Drp1; Fig. 1 A). Mutating the putative phosphate acceptor Thr569 to Ala was without consequence for Drp1-101 localization, dynamics, and mitochondrial morphology. However, the phosphomimetic substitution (T569E) dispersed Drp1-101 from MTs, enhanced its mobility, and induced mitochondrial fragmentation (Fig. 7, B–F). These results confirm the importance of a net positive charge of the MT-binding exon and raise the possibility that Drp1 localization and activity is regulated by phosphorylation at Thr569.

MT localization of Drp1 is cell cycle dependent and regulated by Ser_{CDK} phosphorylation and MT structure

The MT cytoskeleton undergoes dramatic reorganization in dividing cells, and several MT-associated proteins interact specifically

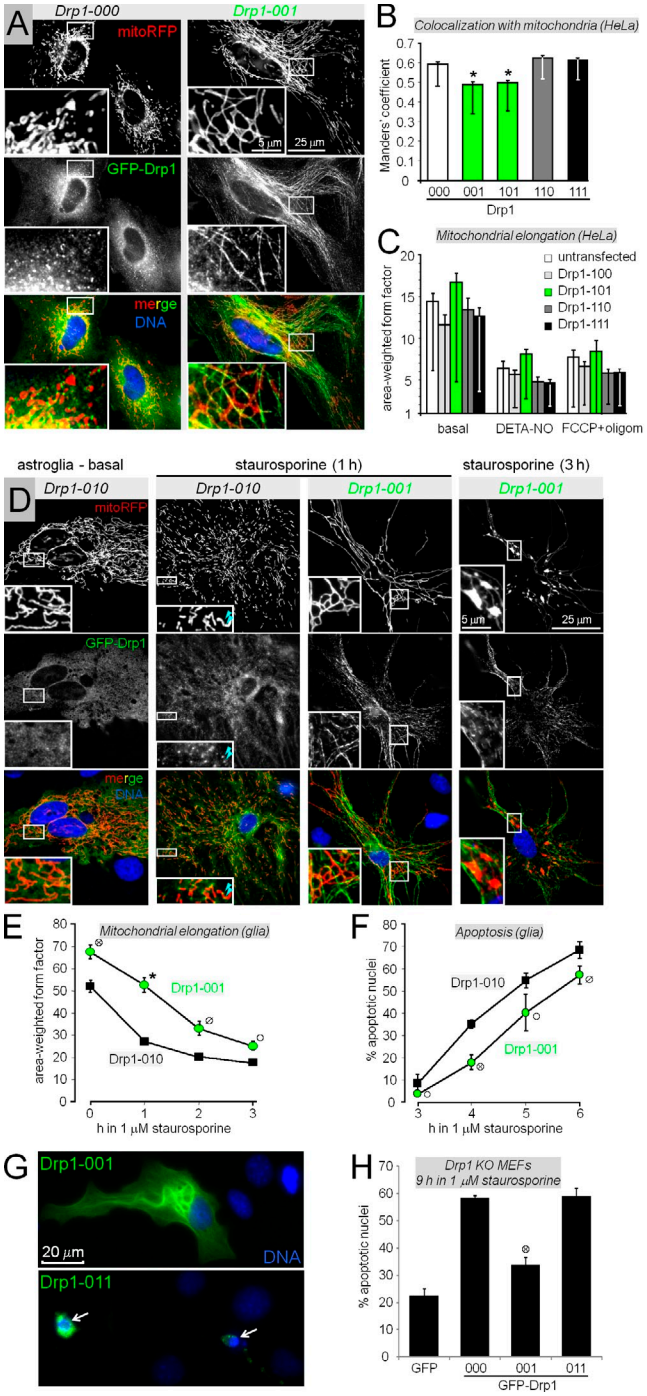

Figure 6. **MT association sequesters Drp1 away from mitochondria and inhibits mitochondrial fission and apoptosis.** (A and B) HeLa cells transfected with mitoRFP and the indicated GFP-Drp1 splice variants were fixed and assessed for colocalization of Drp1 with mitochondria. Representative epifluorescence images are shown in A (means ± SEM [up]/SD [down] of 125–184 cells in B). (C) HeLa cells transfected as indicated and treated with vehicle, the NO donor 2,2′-(hydroxynitrosohydrazono)bis-ethanimine (DETA-NO; 1 mM, 18 h), or the uncoupler carbonylcyanide-p-trifluoromethoxyphenylhydrazone (FCCP; 1 µM, 30 min) in combination with the ATP synthase inhibitor oligomycin (0.1 µM) were immunolabeled for GFP and mitochondria (cytochrome oxidase II) and analyzed for mitochondrial morphology (means ± SEM [up]/SD [down] of ∼100 cells). (D–F) Rat primary astroglia with replacement of endogenous with GFP-Drp1-010 or -001 were treated for up to 6 h with 1 µM staurosporine and scored for shape of mitochondria (mitoRFP) and apoptosis (condensation/fragmentation of nuclei stained with Hoechst 33342). (D) Representative epifluorescence images with arrowheads pointing to Drp1 foci on mitochondria. (E) Mitochondrial morphometry (means ± SEM of 127–140 astrocytes). (F) Counts of apoptotic nuclei (means ± SD of four wells) from representative experiments. (G and H) Drp1 KO MEFs transfected as indicated were challenged with 1 µM staurosporine (9 h) and GFP-positive cells with apoptotic nuclei (arrows [G] were counted [H]; means ± SEM, $n = 3$). ○, $P < 0.05$; ∅, $P < 0.01$; ⊗, $P < 0.0005$; *, $P < 10^{-7}$ compared with all cytosolic Drp1 splice variants.

with either interphase or mitotic MTs (de Forges et al., 2012; Meunier and Vernos, 2012). Rather than colocalizing with the MTs of the spindle apparatus, GFP-Drp1-101 distributed diffusely in mitotic, unsynchronized HeLa cells (prophase through late telophase). MT association commenced again during cytokinesis, when Drp1-101 colocalized prominently with the MT bundles of the midbody (Fig. 8 A). Time-lapse microscopy confirmed that Drp1-x01 transiently dissociates from the MT cytoskeleton during mitosis (Fig. 8 B and Video 2). Next, we examined the localization of endogenous Drp1 by immunofluorescence in asynchronously growing Jurkat cells, which express mostly Drp1-001 (Fig. 2 E and Fig. S1 E). Confirming prior confocal microscopy (Fig. 3, C and D), Drp1 partitioned to both mitochondria and MTs in Jurkat cells during interphase and cytokinesis (Fig. 8 C). Similar to GFP-Drp1-x01 in HeLa cells, endogenous Drp1 in Jurkat cells lost its colocalization with MTs during mitosis as quantified by Pearson's coefficient (Fig. 8, C and D).

Both MTs and Drp1 are postranslationally modified in a cell cycle–dependent manner. In regards to Drp1, Cdk1/cyclin B–mediated phosphorylation at a conserved Ser residue downstream from the C-terminal alternative splice sites (Ser635 in rat Drp1-111 and Ser617 in human Drp1-011—here referred to as Ser_{CDK}) was reported to participate in the breakdown of the mitochondrial reticulum before cell division (Taguchi et al., 2007). Blocking phosphorylation of this site by mutation to Ala was not sufficient to induce association of GFP-Drp1-101 with the mitotic spindle. However, when combined with taxol treatment, $S_{CDK}A$ mutant, but not wild-type Drp1-101, localized robustly to spindle MTs (Fig. 8, E and F). Drp1-x01 is therefore excluded from mitotic MTs by two mechanisms: (1) phosphorylation at Ser_{CDK} and (2) a taxol-sensitive modification of MTs. In contrast to interphase MTs, which often exist as bundles, the mitotic spindle is mostly composed of individual MTs (Meunier and Vernos, 2012). Taxol may therefore recruit Drp1-101 $S_{CDK}A$ to the mitotic spindle by promoting formation of MT bundles, although modifications secondary to MT stabilization, e.g., tubulin acetylation, could also play a role. Consistent with the notion that Drp-x01 not only stabilizes and bundles MTs (Fig. 5) but is also selectively recruited to stable MTs, Drp1-x01 decorates preferentially MT bundles of large caliber, including remnants of the midbody in interphase HeLa cells (Fig. S3).

Association of Drp1-x01 with interphase MTs is modulated by Cdk5 phosphorylation

Because cdk1/cyclin B phosphorylation displaces Drp1-x01 from taxol-stabilized mitotic spindles, we wondered whether Ser_{CDK} phosphorylation may regulate Drp1-x01 localization during interphase as well. Drp1 Ser_{CDK} phosphorylation was partially

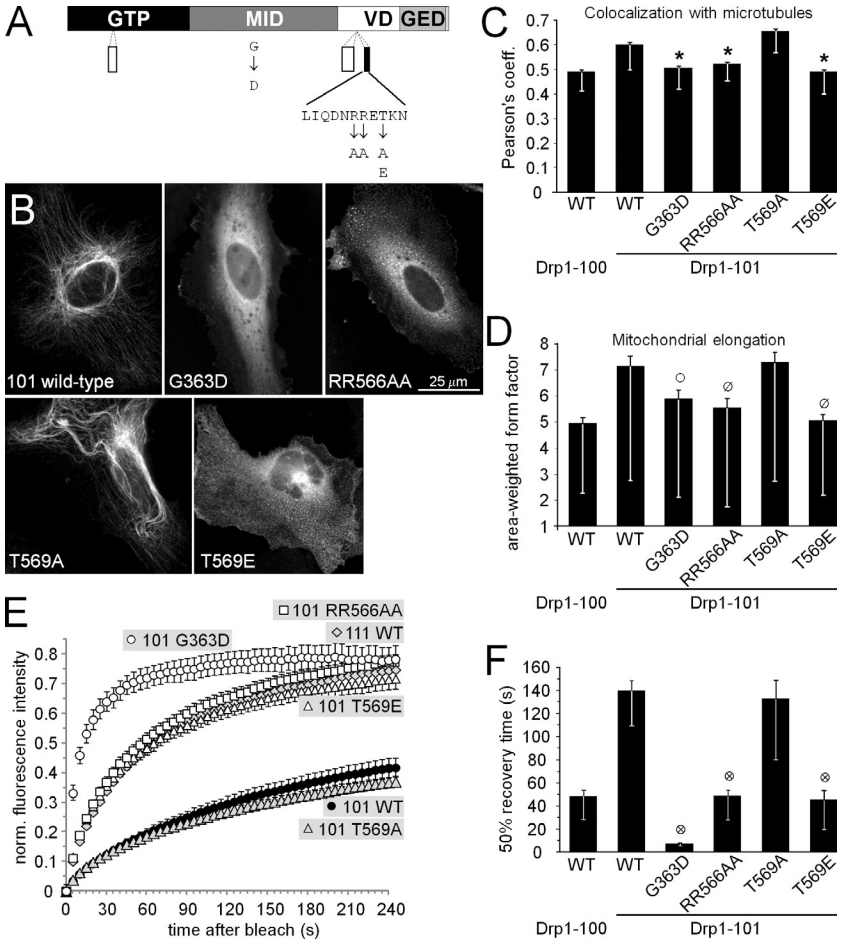

Figure 7. **Molecular determinants for MT association of Drp1.** (A–F) GFP-Drp1 mutants diagrammed in A were substituted into HeLa cells and analyzed for colocalization with MTs (C, α-tubulin immunofluorescence), effects on mitochondrial shape (D, cytochrome oxidase II), and mobility by FRAP (E and F). Shown are epifluorescence images of GFP-Drp1 localization (B), MT colocalization scores (C), mitochondrial morphometry (D; means ± SEM [up]/SD [down] of 124–158 cells), as well as fluorescence recovery curves (E) and their 50% recovery time constants (F; means ± SEM [up]/SD [down] of 7–14 cells) from representative experiments. ○, $P < 0.05$; ∅, $P < 0.001$; ⊗, $P < 10^{-9}$; *, $P < 10^{-11}$ compared with Drp1-101 wild type.

inhibited by roscovitine, a specific Cdk5 inhibitor, but not by pharmacological inhibitors of other proline-directed kinases (JNK, p38, and ERK1/2; unpublished data). Beyond already high basal phosphorylation stochiometry (35–40%; Fig. 2, C and D), forced expression of Cdk5 and its regulatory subunit p35 enhanced Ser_{CDK} phosphorylation levels of both GFP-Drp1-101 and -111 in HeLa cells by about twofold (Fig. 9 A). This number is an underestimate because the commercial phospho-Ser_{CDK} antibody we used has limited cross-reactivity with $S_{CDK}A$ mutant Drp1 (Fig. 9 A). Cdk5/p35 expression also caused redistribution of wild-type Drp1-101 from MTs to the cytosol, whereas $Ser_{CDK}Ala$ mutant Drp1-101 remained MT bound in Cdk5/p35-expressing cells (Fig. 9, B and C). Conversely, inhibition of endogenous Cdk5 with roscovitine (10–25 μM) further increased MT localization of wild-type but had no effect on $Ser_{CDK}Ala$ mutant Drp1-101 (Fig. S4). These results identify cyclin-dependent kinases as regulators of Drp1 localization throughout the cell cycle.

Dynamic instability of MT-bound Drp1 is controlled by Ser_{CDK}

We next explored whether Ser_{CDK} phosphorylation regulates the dynamic exchange between cytosolic and MT-bound pools of Drp1-x01. FRAP experiments showed that blocking phosphorylation ($Ser_{CDK}Ala$) reduced the mobility of Drp1-101 (Fig. 10, A–C; and Fig. S5). Forced expression of Cdk5/p35 greatly enhanced fluorescence recovery of wild-type GFP-Drp1-101 but had no effect on the $Ser_{CDK}Ala$ mutant (Fig. S5). Conversely, roscovitine (10 μM) decreased mobility of wild-type GFP-Drp1-101, whereas the dephospho mutant was refractory to inhibition of endogenous Cdk5 (Fig. 10, A–C).

Wild-type GFP-Drp1-101 often decorated MT bundles discontinuously, whereas the $Ser_{CDK}Ala$ mutant was distributed evenly along bundled MTs (Fig. 10 D). Because cytosolic GFP-Drp1 assembles into spiral-shaped structures around mitochondria (Ingerman et al., 2005; Strack and Cribbs, 2012), we wondered whether Drp1-x01 association with MTs could involve bidirectional growth of a Drp1 polymer from a central nucleation site. Indeed, high-resolution time-lapse video microscopy revealed dynamic instability of wild-type Drp1-101 assemblies, with fluorescence tracks shrinking and expanding at a rate of 0.1–0.2 μm/min, but also catastrophically disassembling into puncta (Fig. 10 D and Video 3). GFP-tagged 4R-tau did not display this behavior, indicating that it reflects Drp1-x01 rather than MT dynamics. To quantify Drp1 polymer dynamics, a motility score was calculated as the mean difference between successive frames of the image series (range 0 to 1). Cdk5 inhibition decreased motility scores of wild-type Drp1-x01 almost to the levels of $Ser_{CDK}Ala$ mutant Drp1-101, a mutant we never observed undergoing catastrophic disassembly (Fig. 10, D and E). These results indicate that cyclin-dependent kinase phosphorylation regulates Drp1 targeting to MTs by shifting the assembly/disassembly equilibrium toward disassembly.

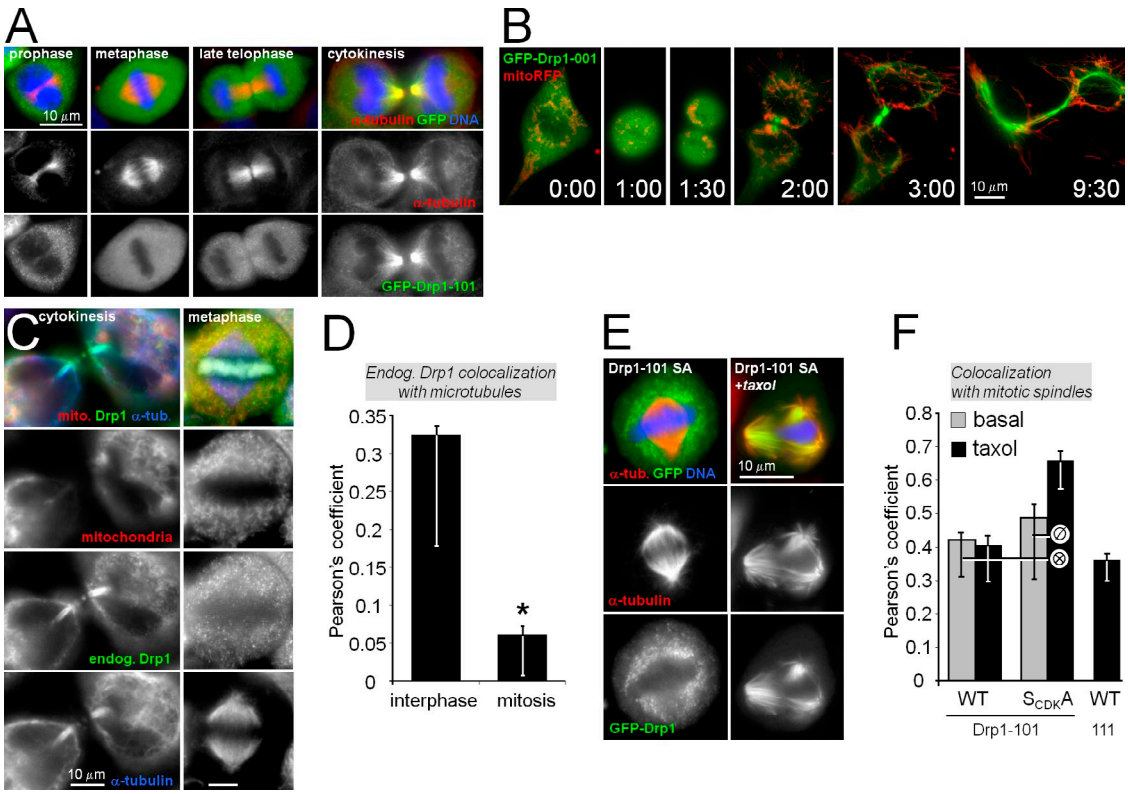

Figure 8. **Ser$_{CDK}$ phosphorylation contributes to dissociation of Drp1-x01 from MTs during mitosis.** (A) GFP-Drp1-101 does not associate with the spindle apparatus in mitotic HeLa cells, but colocalizes with midbody MTs during cytokinesis (representative epifluorescence images of GFP and α-tubulin immunolabeling and Hoechst 33342 DNA staining). (B) Frames from a time-lapse video of a dividing HeLa cell expressing GFP-Drp1-001 and mitoRFP (see also Video 2). (C and D) Colocalization of endogenous Drp1 with α-tubulin and mitochondria (TOM20) in Jurkat cells is lost during mitosis. Representative epifluorescence images are shown in C, whereas Drp1-MT colocalization is quantified as the Pearson's coefficient in D (means ± SEM [up]/SD [down] of 143 and 19 cells). (E and F) HeLa cells expressing the indicated GFP-Drp1 proteins were treated with vehicle or taxol (10 µM, 6 h), processed for immunofluorescence (representative images in C), and analyzed for colocalization of GFP-Drp1 and mitotic spindles (D; means ± SEM of 10–31 cells). ∅, P = 0.006; ⊗, P = 8 × 10^{-6}; *, P = 3 × 10^{-23}.

Discussion

Alternative splicing impacts the endocytosis motor dynamin by multiple mechanisms, including splice-specific association of dynamin-1 with the protein phosphatase calcineurin (Bodmer et al., 2011; Xue et al., 2011). In addition, "long" and "short" forms of Opa1 may have unique roles in apoptosis and inner mitochondrial membrane fusion (Olichon et al., 2007; Song et al., 2007). Here, we show that Drp1 isoforms are functionally distinct and add alternative mRNA splicing to a growing list of regulatory mechanisms that impinge on the mitochondrial fission enzyme (Wilson et al., 2013).

By isoform replacement, we found that Drp1 splice forms including the third but excluding the second alternative exon caused mitochondrial elongation as a consequence of decreased association with the organelle. Consistent with an obligatory role of Drp1-dependent mitochondrial fragmentation in the initiation of apoptosis (Kageyama et al., 2011; Youle and van der Bliek, 2012), Drp1-x01 delayed staurosporine-induced apoptosis in rat primary astroglia and MEFs (Fig. 6). Fractionation and colocalization studies of transfected and endogenous Drp1 indicate that the fission enzyme exists as a heterooligomer in dynamic equilibrium between cytosolic, cytoskeletal, and mitochondrial pools. This equilibrium appears to be regulated by two mechanisms: (1) alternative splicing dictating relative Drp1-x01 expression levels, with 50% representing a threshold for detectable MT association and (2) reversible phosphorylation. Specifically, MT association is blocked by Drp1 phosphorylation at a conserved Ser residue in the constant portion of the variable domain, with phosphorylation by Cdk1 and Cdk5 contributing, respectively, to Drp1-x01 dissociation from the spindle apparatus during mitosis (Fig. 8, C and D) and from the interphase MT cytoskeleton (Fig. 9). In agreement with a previous study (Cereghetti et al., 2008), we were unable to establish a role for Ser$_{CDK}$ in the context of two cytosolic Drp1 splice variants. Because this site is highly phosphorylated in all Drp1 isoforms (Fig. 2, C and D), Ser$_{CDK}$ therefore appears to regulate Drp1 function in a splice-specific manner.

Vallee and co-workers initially purified dynamin-1 from a MT-associated protein fraction and named it alluding to the MT motor protein dynein (Shpetner and Vallee, 1989; Obar et al., 1990). More recently, dynamin-2 was shown to bind mitotic MTs to regulate cell cycle progression in an apparent phosphorylation-dependent manner (Thompson et al., 2004; Tanabe and Takei, 2009; Morita et al., 2010; Ishida et al., 2011). Phospho-regulated MT association may therefore be a common feature among cytosolic dynamin-family GTPases. Whereas dynamin-2 was reported to interact with the highly dynamic MTs of the mitotic spindle and to promote dynamic instability of interphase MTs (Tanabe

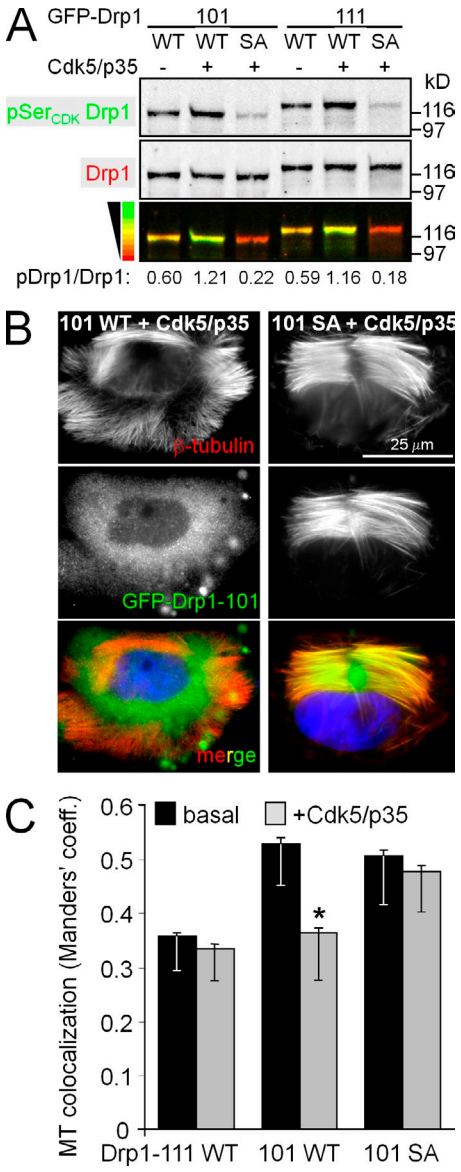

Figure 9. **Cdk5 phosphorylates Drp1 at Ser$_{CDK}$ to disrupt MT targeting of Drp1-x01.** (A) GFP-Drp1-101/111 wild type (WT) and Ser$_{CDK}$Ala (SA) mutant was coexpressed ± Cdk5/p35 in HeLa cells and total lysates were analyzed for Drp1 Ser$_{CDK}$ phosphorylation with a phospho-preferring antibody. The ratio of phosphorylated (pDrp1) to total Drp1 is listed in arbitrary units. (B and C) HeLa cells expressing GFP-Drp1 ± Cdk5/p35 were treated with taxol (10 µM, 6 h) and analyzed for colocalization of GFP and β-tubulin immunofluorescence signals. Representative epifluorescence images are shown in B, whereas colocalization scores are plotted in C (means ± SEM [up]/SD [down] of 53–108 cells). *, P = 10^{-22} comparing Drp1-101 wild type ± Cdk5/p35.

and Takei, 2009; Ishida et al., 2011), we report here that Drp1-x01 dissociates from MTs during mitosis (Fig. 8 and Video 2) and that Drp1-x01 expression enhanced the formation of stable, acetylated MT bundles and slowed fluorescence recovery of α-tubulin in interphase HeLa cells (Fig. 5). Drp1-x01 may thus have dual functions as a membrane severing mechanoenzyme and as a MT-stabilizing protein akin to tau, MAP2, and MAP4 (Dehmelt and Halpain, 2005; de Forges et al., 2012).

At both mRNA and protein levels, MT-targeted Drp1-001 is a major isoform in common laboratory cell lines and predominates in Jurkat T cells, human white blood cells, and several nonneuronal tissues, contributing up to 90% of total Drp1 in spleen and thymus (Fig. S1 E and Fig. 2, A and B). Although the evolutionary significance of the enrichment of Drp1-001 in immune cells requires further investigation, our results indicate that in cells with ≥50% Drp1-x01, Drp1 oligomers compartmentalize to cytosol, mitochondria, and MTs (Fig. 10 F). Upon Ser$_{CDK}$ phosphorylation, Drp1-x01 is liberated from the MT cytoskeleton, so it can join other Drp1 isoforms to cycle between cytosolic and mitochondrial pools and divide the organelle. Upon dephosphorylation by calyculin A–sensitive phosphatases (Fig. 2 D), Drp1-x01 reassociates with MTs, leading to elongation of mitochondria by unopposed fusion.

In addition to inducing MT stabilization and bundling, Drp1-x01 preferentially colocalizes with large-caliber MT bundles that approximate the diameter of mitochondria (Fig. S3), and MTs of the mitotic spindle recruit Drp1 only after bundling by taxol (Fig. 8, E and F). In addition, MT-associated Drp1 forms extended assemblies that expand and shrink, as well as abruptly disintegrate into puncta (Fig. 10, D and E; and Video 3). Together, these observations suggest that Drp1 localizes to MTs and mitochondria by similar mechanisms (Fig. 10 F). Specifically, we propose that MT bundles can serve as templates for the assembly of Drp1 spirals similar in diameter and pitch to those encircling mitochondria. However, MT-ensheathing Drp1 spirals can grow considerably longer, presumably because MT bundles resist Drp1's GTPase-powered constrictive force that would sever a mitochondrion. Whereas Drp1 is recruited to mitochondria via OMM-anchored receptor proteins, we further propose that Drp1-x01 spirals are stabilized via direct, electrostatic interactions between conserved basic residues in the third alternative exon (Arg566/567; Fig. 7) and the acidic N termini of α/β-tubulin, an interaction mechanism shared with tau and other MT-associated proteins (Downing, 2000; Dehmelt and Halpain, 2005). Drp1-x11 is cytosolic despite the presence of the third alternative exon, because residues encoded by the second alternative exon may physically occlude or counterbalance the positive charge of the adjacent MT binding domain. Similarly, phosphorylation at Ser$_{CDK}$ in the constant portion of the variable domain could overcome Arg566 and Arg567 to displace Drp1-x01 from MTs by electrostatic repulsion. Because Mff binds to the stalk domain of Drp1 (Strack and Cribbs, 2012), Drp1 recruitment to mitochondria is influenced by alternative splicing and phosphorylation in the variable domain only indirectly, i.e., via competition with MTs (Fig. 10 G).

The mechanism of action we report for Ser$_{CDK}$ phosphorylation is distinct from phosphorylation of Drp1 at Ser$_{PKA}$, a site at the N-terminal border of the C-terminal GTPase effector 21 residues downstream of Ser$_{CDK}$. PKA targets this site to inhibit Drp1 activity by, depending on whether phosphorylation occurs in the cytosol or at the OMM, either retaining the fission enzyme in the cytosol (Cereghetti et al., 2008) or by promoting the accumulation of nonproductive Drp1 complexes at the OMM (Merrill et al., 2011). Predicted to be in proximity to one of the two Drp1 oligomerization interfaces, Ser$_{PKA}$ phosphorylation appears to inhibit the formation of short oligomers in the cytosol and of functional spirals at the OMM (Strack and Cribbs, 2012).

In conclusion, our results suggest that alternative splicing generates a cytoskeletal "reserve pool" of Drp1 that can be

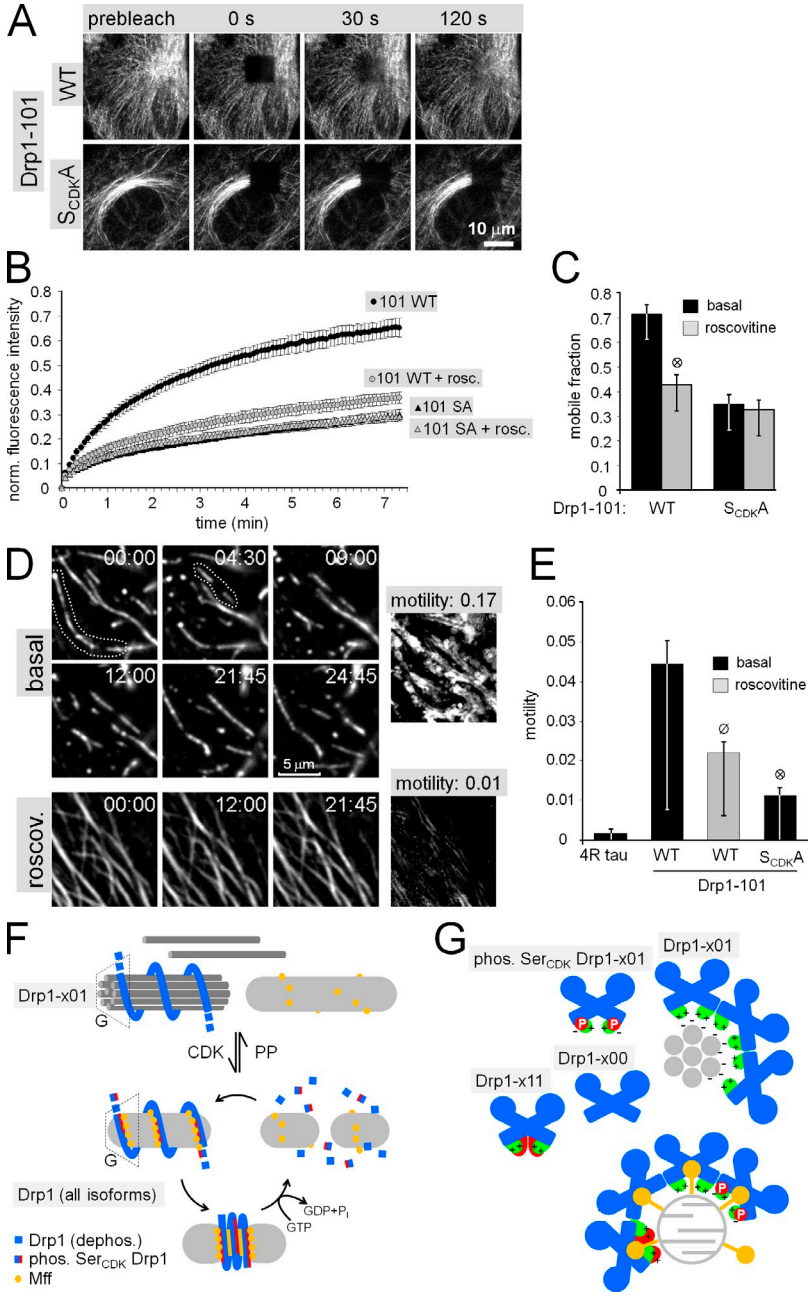

Figure 10. **Ser_{CDK} phosphorylation promotes dynamic instability of MT-associated Drp1.** (A–C) Cdk5 inhibition by roscovitine (10 µM) attenuates fluorescence recovery of wild-type Drp1-101, but has no effect on the Ser_{CDK}Ala mutant. (A) shows time frames of FRAP in representative HeLa cells expressing wild-type and Ser_{PKA}Ala GFP-Drp1-101, recovery curves (B), and mobile fractions (C) derived from biexponential fits of the recovery data (means ± SEM [up]/SD [down] of 6–8 cells). (D and E) Time-lapse video microscopy of HeLa cells expressing the indicated GFP-tagged proteins shows that Drp1-101 polymers shrink and expand in a Cdk5- and Ser_{CDK}-dependent manner (see also Video 3). (D, left) Time frames of representative cells, with dotted outlines marking Drp1-x01 tracks about to undergo shrinkage or expansion. (D, right) Mean z-projections of inter-frame difference images from which motility indices (0–1) are calculated (E; means ± SEM [up]/SD [down] of 31–41 whole cells). ∅, P = 0.001; ⊗, P < 0.0001 compared with Drp1-101 wild-type basal. (F and G) Models of regulated MT association of Drp1 (see text).

mobilized by cyclin-dependent kinase phosphorylation. However, given that MTs are critically involved in localizing mitochondria, as well as in orchestrating both fission and fusion events (Varadi et al., 2004; Bowes and Gupta, 2008; Jourdain et al., 2009; Saxton and Hollenbeck, 2012), it is also conceivable that cytoskeletal Drp1 plays more active roles, for instance, by facilitating highly localized mitochondrial membrane remodeling. Such roles may not even involve mitochondria, as indicated by the ability of Drp1-x01 to modulate MT dynamics.

Materials and methods

Plasmids, cells, and antibodies

Plasmids coexpressing H1 promoter–driven shRNA to silence endogenous Drp1 as well as GFP- or 3× HA-tagged, RNAi-resistant Drp1 (rat 111 splice variant; GenBank accession no. AF019043) were described previously (Cribbs and Strack, 2007). Plasmids are based on pEGFP-C1 (Takara Bio Inc.), with the Drp1 coding sequence ligated via BamHI and EcoRI sites, and the H1 promoter shRNA cassette ligated via PciI sites. To generate 3HA-Drp1, the EGFP coding sequence was excised via AgeI and BspEI sites and replaced with the sequence encoding three HA tags. Other Drp1 splice variants were generated by deletion mutagenesis from Drp1-111 according to the QuikChange protocol (Agilent Technologies). Point mutants were made by the same protocol. The GFP-4R-tau and α-tubulin-EYFP plasmids were provided by G. Lee (University of Iowa, Iowa City, IA) and M. Horne (University of California, Davis, Davis, CA), respectively. Drp1 KO MEFs were a gift of H. Sesaki (Johns Hopkins University, Baltimore, MD) and Jurkat 6E.1 cells and PBMCs were provided by J. Houtman (University of Iowa, Iowa City, IA). Antibodies against the following antigens were obtained commercially: GFP (rabbit; Abcam); HA (mouse; Santa Cruz Biotechnology, Inc.); Drp1 and PP2A/C subunit (mouse; BD); cytochrome oxidase subunit II (mouse; Neomarkers); TOM40 (rabbit; Santa Cruz Biotechnology, Inc.); TOM20 (rabbit; Santa Cruz Biotechnology, Inc.); α-tubulin (goat; Santa Cruz Biotechnology, Inc.); β-tubulin (mouse, E3; Developmental Studies Hybridoma Bank); tyrosinated α-tubulin (rat, YL1/2; Abcam); and acetylated α-tubulin (mouse, 6-11B-1; Santa Cruz Biotechnology, Inc.).

Rabbit polyconal antibodies specific for the Drp1-x01 isoform were raised against the exon-spanning peptide acetyl-SRDKLIQDNRR-C, which was coupled to maleimide-activated keyhole limpet hemocyanine (Thermo Fisher Scientific) via its C-terminal Cys residue. Antibodies were purified using a peptide affinity column according to the manufacturer's instructions (UltraLink iodoacetyl gel; Thermo Fisher Scientific).

qRT-PCR

Total RNA was extracted from cells and tissues using TRIzol reagent as per the manufacturer's instructions (Invitrogen). qRT-PCR was performed using the SYBR Green One-Step RT-PCR kit (QIAGEN) on a Touch Real-Time PCR detection system (CFX96; Bio-Rad Laboratories). The following primers were used to amplify 136–199-bp Drp1 splice form–specific amplicons: N-terminal exon: Drp1-N forward, 5′-GGAAAGAGCTCAGTGCTGGAAAGCC-3′; Drp1-0xx reverse, 5′-CCATTCTTCTGCTTCAACTCCATTTTC-3′; Drp1-1xx reverse, 5′-CCCATTCTTCTGCTTCAACTCCTTTAG-3′; C-terminal exons: Drp1-C forward, 5′-GCTGATGCCTGTGGGCTAATGAAC-3′; Drp1-x00 reverse, 5′-CACCTGCAGATGCAACCTTGTCTCG-3′; Drp1-x01 reverse, 5′-CTGTTGTCCTGAATTAACTTGTCTCG-3′; Drp1-x10 reverse, 5′-CACCTGCAGATGCAACCTTGCCATC-3′; Drp1-x11 reverse, 5′-CTGCTGTCCTGAATTAACTTGCCATC-3′. Drp1 splice form levels were quantified using the $\Delta\Delta C_t$ method, using phosphoglycerate kinase 1 (Pgk1) mRNA as an internal standard (Pgk1 forward, 5′-CTGGAGAACCTCCGCTTTCATG-3′; Pgk1 reverse, 5′-CAAAAGCATCATTGACATAGACATC-3′).

2D PAGE and immunoblotting

To dephosphorylate cellular proteins, ~2×10^6 cells were lysed in 100 µl hypotonic solution (0.5% Triton X-100, 0.5 mM EDTA, 0.5% ampholytes, pH 3–10, 1 mM phenylmethylsulfonyl fluoride, 5 µg/ml leupeptin, and 1 mM benzamidine) and incubated (30 min, 30°C) with calf intestinal alkaline phosphatase (50 U/ml; New England Biolabs, Inc.). Control extracts were incubated minus alkaline phosphatase plus 1 µM microcystin LR to prevent dephosphorylation by endogenous phosphatases. After addition of 3 vol of isoelectric focusing (IEF) sample buffer (7 M urea, 2 M thiourea, 1.25% CHAPS, 32 mM DTT, 2.5 mM tris(2-carboxyethyl)phosphine, 0.5% amidosulfobetain-14, 0.5% Triton X-100, 0.5% Zwittergent 3–10, and 0.8% ampholytes, pH 3–10), lysates were cleared by centrifugation (10 min at 20,000 *g*). For other experiments, cells were directly lysed in IEF sample buffer.

Immobilized pH gradient strips (11 cm, pH 5–8; Bio-Rad Laboratories) were equilibrated (14–20 h, 25°C) with 225 µl of cleared lysate (500–800 µg of protein), followed by IEF for 20,000 Vxh. After IEF, strips were incubated (15 min, 25°C) in equilibration buffer (2% SDS, 6 M urea, 20% [vol/vol] glycerol, 50 mM Tris, pH 8.8, and trace bromophenol blue) including 50 mM DTT, followed by a second incubation in equilibration buffer plus 100 mM iodoacetamide to block free sulfhydryls. Proteins were then separated according to molecular weight on 10% polyacrylamide gels and transferred to nitrocellulose (60 min at 1 A in 10 mM N-cyclohexyl-3-aminopropanesulfonic acid, pH 11, and 10% methanol). After blocking in 2% bovine serum albumin, membranes were incubated with appropriate primary and infrared dye-coupled secondary antibodies and imaged using an Odyssey infrared laser scanner (LI-COR Biosciences). ImageJ software was used for band and spot densitometry (Collins, 2007; Schneider et al., 2012). Blots shown were processed by linear auto-contrast enhancement.

MT purification

Cells were lysed (10 min, 25°C) in PHEM buffer (10 mM EGTA, 2 mM $MgCl_2$, 60 mM Pipes, and 25 mM Hepes, pH 6.9) including 0.2% Triton X-100, 1 mM benzamidine, 1 mM PMSF, 1 mM DTT, 5 µg/ml leupeptin, 2 µg/ml pepstatin, 1 mM GTP, and bromophenol blue (trace) either in the presence or absence of 10 µM taxol. Lysates were layered on top of 1 M sucrose in PHEM buffer containing 1 mM PMSF, 1 mM DTT, 5 µg/ml leupeptin, 2 µg/ml pepstatin, and 1 mM GTP ± 10 µM taxol and centrifuged (20,000 *g*, 2 min, 25°C). After aspiration of the supernatant, pellets were dissolved in SDS sample buffer and analyzed by SDS-PAGE.

Fluorescence microscopy and image analysis

HeLa cells, rat primary astroglia, and MEFs were cultured on chambered No. 1 cover glasses (20-mm^2 chamber; Thermo Fisher Scientific) and transfected using Lipofectamine 2000. 24–48 h later, cells were fixed with 4% paraformaldehyde in PBS. For experiments involving cotransfection of mitoRFP (dsRed2/mito; Takara Bio Inc.) and GFP-Drp1 (1:3 plasmid weight ratio), cells were imaged after brief staining with 1 µg/ml Hoechst 33342 to label nuclei. When only GFP-Drp1 was transfected, cells were subjected to immunofluorescence staining with antibodies to cytochrome oxidase II (HeLa cells only), α- or β-tubulin, and GFP. After incubation with Alexa Fluor–coupled secondary antibodies (488, 555, or 633; Invitrogen) and Hoechst 33342 (1 µg/ml), digital images were captured using a epifluorescence microscope (63×, NA 1.4, or 100×, NA 1.4, oil immersion lens; DMI4000B; Leica) with a camera (DFC350FX) and LAF acquisition software (Leica). Cells were imaged in PBS at 25°C. To avoid overexpression artifacts (e.g., nonmitochondrial puncta seen mostly with cytosolic Drp1 splice variants), only cells with intermediate GFP-Drp1 levels were analyzed. According to quantitative immunofluorescence analysis, GFP-Drp1 isoforms were expressed to 230–320% of endogenous Drp1 in HeLa cells and to 120–190% in Drp1 KO MEFs. Using custom-written macros (see online supplemental material) and plugins for ImageJ (Cribbs and Strack, 2009), images were deblurred by iterative deconvolution with a computed point spread function and analyzed for channel colocalization and mitochondrial morphology. For the former, the JoCoP plugin was used to report Manders' and Pearson's coefficients (Bolte and Cordelières, 2006). For morphometry, mitochondria channels were auto-segmented and subjected to ImageJ's Analyze Particles function, extracting major and minor axis, area, and perimeter (p). Area-weighted form factor ($p^2/4\pi$) was calculated for each mitochondrial object and then averaged across a region of interest (usually a cell). This metric has a minimum value of one for circular objects and is particularly sensitive to increases in mitochondrial length and interconnectivity from already elongated mitochondria as found in HeLa cells and primary astrocytes (Merrill et al., 2011). Mitochondrial length was determined by first applying ImageJ's Skeletonize function to the auto-segmented image to reduce mitochondria to single-pixel-width lines, and then applying Analyze Particles to extract length as area.

For morphometry of MT bundles, tubulin immunofluorescence images were auto-segmented and subjected to the Analyze Particles function as described in the previous paragraph. The ratio of area to perimeter of the cellular MT cytoskeleton robustly increases upon brief taxol exposure (2 µM, 30 min) and is reported here as the MT bundling index. Epifluorescence images shown are either unprocessed or subjected to linear auto-contrast enhancement using either Photoshop CS3 or ImageJ.

FRAP

FRAP was performed as reported previously (Merrill et al., 2011) with minor modifications. In brief, HeLa cells were cultured in 10% fetal bovine serum in DMEM/F12 (without phenol red and buffered with 20 mM Hepes, pH 7.4) on collagen-coated, chambered No. 1 cover glasses (Thermo Fisher Scientific) and transfected with GFP-Drp1 or mCherry-Drp1 plus EYFP-α-tubulin using Lipofectamine 2000 the day before analysis. Using the 488-nm laser line of a laser scanning confocal microscope (LSM 510; Carl Zeiss) an approximately 10 × 10-µm region of cytosol was bleached and fluorescence recovery was recorded by capturing images every 5 s for 5 to 8 min using LSM 4.2 acquisition software and a 63× oil immersion lens (NA 1.4) at 25°C. Image stacks were analyzed and recovery curves normalized to prebleach intensity and corrected for acquisition bleach (McNally, 2008) were approximated by single and double exponential recovery equations using a custom-written ImageJ macro (see online supplemental material), yielding 50% recovery time constant ($t_{1/2}$) and mobile fraction. Drp1 dynamics followed double exponential recovery kinetics with R^2 values of generally >0.99. Confocal images shown are either unprocessed or subjected to linear auto-contrast enhancement using ImageJ.

Time-lapse video microscopy

For live imaging, HeLa cells were maintained in 10% fetal bovine serum in DMEM/F12 without phenol red and buffered with 20 mM Hepes, pH 7.4. To monitor Drp1-x01 dynamics during the cell cycle, cells were cotransfected with GFP-Drp1 and mitoRFP (dsRed2/mito; Takara Bio Inc.) and subjected to time-lapse video microscopy using the 40× oil immersion objective (1.35 NA) of a motorized epifluorescence microscope (IX81; Olympus) under temperature (37°C), CO_2 (5%), and humidity control. Images were captured every 30 min for 20 h using an Orca-ER camera (Hamamatsu Photonics) and SlideBook 5.0 acquisition software (Intelligent Imaging Innovations, Inc.). To visualize Drp1-x01 dynamics on MTs, transfected cells were imaged using the 63× (NA 1.4) objective of a motorized epifluorescence microscope (DMI6000B; Leica) under temperature (37°C), CO_2 (5%), and humidity control. Images were captured every 15 s for up to 40 min using a DFC345FX camera and LAF acquisition software (Leica). Using a custom-written macro for ImageJ software (see online supplemental material), image series were auto-contrasted, and Drp1 dynamics was quantified as a motility index (MI), which varies between 0 and 1 and represents the mean difference between consecutive frames of the time-lapse series. For example, the MI of the first two frames is $MI_{(1,2)}$ = mean{subtract[difference(frame1,frame2),Th]}/mean{subtract[max(frame1,frame2),Th]}, where *subtract*, *difference*, and *max* are operators in ImageJ's Image Calculator

function, and *mean* is the resulting image's mean pixel intensity. *Th* (threshold) is a constant that reduces the effects of image noise and spurious intensity fluctuations (1/8 of maximum pixel intensity by default).

Statistical analysis

Data were analyzed by Student's *t* test (two-tailed, unequal variance) for single comparisons and by one- or two-way analysis of variance (ANOVA) for multiple comparisons. For multiple comparisons to a single (reference) dataset, ANOVA was followed by the Dunnett post-test; otherwise, we used pairwise *t* tests with Bonferroni adjustment. Datasets approximated normal (Gaussian) distribution, except for mitochondrial morphology metrics, which followed a log-normal (right skewed) distribution and required log transformation before parametric tests. A subset of the data, including mitochondrial morphology, was also analyzed by nonparametric tests (Mann-Whitney *U* test and Kruskal-Wallis one-way ANOVA), confirming significances. All data shown are representative of at least three independent experiments.

Online supplemental material

Fig. S1 shows rescue of mitochondrial fission in Drp1 KO MEFs, Drp1 mRNA profiling in primary cells and cell lines, and Drp1-x01 antibody characterization. Fig. S2 shows that mixed oligomeric assembly of Drp1 splice forms modulates MT targeting. Fig. S3 shows that Drp1-001 preferentially decorates large caliber MT bundles. Fig. S4 shows that Cdk5 inhibition by roscovitine enhances MT targeting of Drp1-101. Fig. S5 shows that Cdk5/p35 overexpression promotes Drp1-101 dynamics. Video 1 shows fluorescence recovery of Drp1 splice variants and tau. Video 2 shows Drp1-x01 localization during the cell cycle. Video 3 shows dynamic instability of Drp1-x01. ImageJ macros for batch processing of microscope images and experimental analysis are also provided. Online supplemental material is available at http://www.jcb.org/cgi/content/full/jcb.201210045/DC1.

We thank Gloria Lee, Hiromi Sesaki, Mary Horne, and Jon Houtman for reagents and advice and Andrew Slupe for help with statistical analyses using R software. We are also grateful for services by the Central Microscopy Research Facility (University of Iowa) and the Hybridoma Facility (Iowa State University).

This work was supported by National Institutes of Health grants NS056244 and NS057714 to S. Strack.

Submitted: 9 October 2012
Accepted: 16 May 2013

References

Bodmer, D., M. Ascaño, and R. Kuruvilla. 2011. Isoform-specific dephosphorylation of dynamin1 by calcineurin couples neurotrophin receptor endocytosis to axonal growth. *Neuron*. 70:1085–1099. http://dx.doi.org/10.1016/j.neuron.2011.04.025

Bolte, S., and F.P. Cordelières. 2006. A guided tour into subcellular colocalization analysis in light microscopy. *J. Microsc.* 224:213–232. http://dx.doi.org/10.1111/j.1365-2818.2006.01706.x

Bowes, T., and R.S. Gupta. 2008. Novel mitochondrial extensions provide evidence for a link between microtubule-directed movement and mitochondrial fission. *Biochem. Biophys. Res. Commun.* 376:40–45. http://dx.doi.org/10.1016/j.bbrc.2008.08.120

Cereghetti, G.M., A. Stangherlin, O. Martins de Brito, C.R. Chang, C. Blackstone, P. Bernardi, and L. Scorrano. 2008. Dephosphorylation by calcineurin regulates translocation of Drp1 to mitochondria. *Proc. Natl. Acad. Sci. USA*. 105:15803–15808. http://dx.doi.org/10.1073/pnas.0808249105

Chang, C.R., and C. Blackstone. 2007. Cyclic AMP-dependent protein kinase phosphorylation of Drp1 regulates its GTPase activity and mitochondrial morphology. *J. Biol. Chem.* 282:21583–21587. http://dx.doi.org/10.1074/jbc.C700083200

Chang, C.R., C.M. Manlandro, D. Arnoult, J. Stadler, A.E. Posey, R.B. Hill, and C. Blackstone. 2010. A lethal de novo mutation in the middle domain of the dynamin-related GTPase Drp1 impairs higher order assembly and mitochondrial division. *J. Biol. Chem.* 285:32494–32503. http://dx.doi.org/10.1074/jbc.M110.142430

Chen, H., S.A. Detmer, A.J. Ewald, E.E. Griffin, S.E. Fraser, and D.C. Chan. 2003. Mitofusins Mfn1 and Mfn2 coordinately regulate mitochondrial fusion and are essential for embryonic development. *J. Cell Biol.* 160:189–200. http://dx.doi.org/10.1083/jcb.200211046

Collins, T.J. 2007. ImageJ for microscopy. *Biotechniques*. 43:25–30. http://dx.doi.org/10.2144/000112517

Cribbs, J.T., and S. Strack. 2007. Reversible phosphorylation of Drp1 by cyclic AMP-dependent protein kinase and calcineurin regulates mitochondrial fission and cell death. *EMBO Rep.* 8:939–944. http://dx.doi.org/10.1038/sj.embor.7401062

Cribbs, J.T., and S. Strack. 2009. Functional characterization of phosphorylation sites in dynamin-related protein 1. *Methods Enzymol.* 457:231–253. http://dx.doi.org/10.1016/S0076-6879(09)05013-7

Davies, V.J., A.J. Hollins, M.J. Piechota, W. Yip, J.R. Davies, K.E. White, P.P. Nicols, M.E. Boulton, and M. Votruba. 2007. Opa1 deficiency in a mouse model of autosomal dominant optic atrophy impairs mitochondrial morphology, optic nerve structure and visual function. *Hum. Mol. Genet.* 16:1307–1318. http://dx.doi.org/10.1093/hmg/ddm079

de Forges, H., A. Bouissou, and F. Perez. 2012. Interplay between microtubule dynamics and intracellular organization. *Int. J. Biochem. Cell Biol.* 44:266–274. http://dx.doi.org/10.1016/j.biocel.2011.11.009

Dehmelt, L., and S. Halpain. 2005. The MAP2/Tau family of microtubule-associated proteins. *Genome Biol.* 6:204. http://dx.doi.org/10.1186/gb-2004-6-1-204

Downing, K.H. 2000. Structural basis for the interaction of tubulin with proteins and drugs that affect microtubule dynamics. *Annu. Rev. Cell Dev. Biol.* 16:89–111. http://dx.doi.org/10.1146/annurev.cellbio.16.1.89

Faelber, K., Y. Posor, S. Gao, M. Held, Y. Roske, D. Schulze, V. Haucke, F. Noé, and O. Daumke. 2011. Crystal structure of nucleotide-free dynamin. *Nature*. 477:556–560. http://dx.doi.org/10.1038/nature10369

Ford, M.G., S. Jenni, and J. Nunnari. 2011. The crystal structure of dynamin. *Nature*. 477:561–566. http://dx.doi.org/10.1038/nature10441

Frank, S., B. Gaume, E.S. Bergmann-Leitner, W.W. Leitner, E.G. Robert, F. Catez, C.L. Smith, and R.J. Youle. 2001. The role of dynamin-related protein 1, a mediator of mitochondrial fission, in apoptosis. *Dev. Cell*. 1:515–525. http://dx.doi.org/10.1016/S1534-5807(01)00055-7

Hammond, J.W., D. Cai, and K.J. Verhey. 2008. Tubulin modifications and their cellular functions. *Curr. Opin. Cell Biol.* 20:71–76. http://dx.doi.org/10.1016/j.ceb.2007.11.010

Hoppins, S., L. Lackner, and J. Nunnari. 2007. The machines that divide and fuse mitochondria. *Annu. Rev. Biochem.* 76:751–780. http://dx.doi.org/10.1146/annurev.biochem.76.071905.090048

Howng, S.L., W.D. Sy, T.S. Cheng, A.S. Lieu, C. Wang, W.S. Tzou, C.L. Cho, and Y.R. Hong. 2004. Genomic organization, alternative splicing, and promoter analysis of human dynamin-like protein gene. *Biochem. Biophys. Res. Commun.* 314:766–772. http://dx.doi.org/10.1016/j.bbrc.2003.12.172

Ingerman, E., E.M. Perkins, M. Marino, J.A. Mears, J.M. McCaffery, J.E. Hinshaw, and J. Nunnari. 2005. Dnm1 forms spirals that are structurally tailored to fit mitochondria. *J. Cell Biol.* 170:1021–1027. http://dx.doi.org/10.1083/jcb.200506078

Ishida, N., Y. Nakamura, K. Tanabe, S.A. Li, and K. Takei. 2011. Dynamin 2 associates with microtubules at mitosis and regulates cell cycle progression. *Cell Struct. Funct.* 36:145–154. http://dx.doi.org/10.1247/csf.10016

Ishihara, N., M. Nomura, A. Jofuku, H. Kato, S.O. Suzuki, K. Masuda, H. Otera, Y. Nakanishi, I. Nonaka, Y. Goto, et al. 2009. Mitochondrial fission factor Drp1 is essential for embryonic development and synapse formation in mice. *Nat. Cell Biol.* 11:958–966. http://dx.doi.org/10.1038/ncb1907

Jourdain, I., Y. Gachet, and J.S. Hyams. 2009. The dynamin related protein Dnm1 fragments mitochondria in a microtubule-dependent manner during the fission yeast cell cycle. *Cell Motil. Cytoskeleton*. 66:509–523. http://dx.doi.org/10.1002/cm.20351

Kageyama, Y., Z. Zhang, and H. Sesaki. 2011. Mitochondrial division: molecular machinery and physiological functions. *Curr. Opin. Cell Biol.* 23:427–434. http://dx.doi.org/10.1016/j.ceb.2011.04.009

Koch, A., M. Thiemann, M. Grabenbauer, Y. Yoon, M.A. McNiven, and M. Schrader. 2003. Dynamin-like protein 1 is involved in peroxisomal fission. *J. Biol. Chem.* 278:8597–8605. http://dx.doi.org/10.1074/jbc.M211761200

McNally, J.G. 2008. Quantitative FRAP in analysis of molecular binding dynamics in vivo. *Methods Cell Biol.* 85:329–351. http://dx.doi.org/10.1016/S0091-679X(08)85014-5

Merrill, R.A., R.K. Dagda, A.S. Dickey, J.T. Cribbs, S.H. Green, Y.M. Usachev, and S. Strack. 2011. Mechanism of neuroprotective mitochondrial remodeling by PKA/AKAP1. *PLoS Biol.* 9:e1000612. http://dx.doi.org/10.1371/journal.pbio.1000612

Meunier, S., and I. Vernos. 2012. Microtubule assembly during mitosis - from distinct origins to distinct functions? *J. Cell Sci.* 125:2805–2814. http://dx.doi.org/10.1242/jcs.092429

Morita, M., K. Hamao, S. Izumi, E. Okumura, K. Tanaka, T. Kishimoto, and H. Hosoya. 2010. Proline-rich domain in dynamin-2 has a low microtubule-binding activity: how is this activity controlled during mitosis in HeLa cells? *J. Biochem.* 148:533–538. http://dx.doi.org/10.1093/jb/mvq116

Morlot, S., and A. Roux. 2013. Mechanics of Dynamin-Mediated Membrane Fission. *Annu Rev Biophys*.

Obar, R.A., C.A. Collins, J.A. Hammarback, H.S. Shpetner, and R.B. Vallee. 1990. Molecular cloning of the microtubule-associated mechanochemical

enzyme dynamin reveals homology with a new family of GTP-binding proteins. *Nature*. 347:256–261. http://dx.doi.org/10.1038/347256a0

Olichon, A., G. Elachouri, L. Baricault, C. Delettre, P. Belenguer, and G. Lenaers. 2007. OPA1 alternate splicing uncouples an evolutionary conserved function in mitochondrial fusion from a vertebrate restricted function in apoptosis. *Cell Death Differ.* 14:682–692. http://dx.doi.org/10.1038/sj.cdd.4402048

Otera, H., N. Ishihara, and K. Mihara. 2013. New insights into the function and regulation of mitochondrial fission. *Biochim. Biophys. Acta*. 1833:1256–1268. http://dx.doi.org/10.1016/j.bbamcr.2013.02.002

Pitts, K.R., Y. Yoon, E.W. Krueger, and M.A. McNiven. 1999. The dynamin-like protein DLP1 is essential for normal distribution and morphology of the endoplasmic reticulum and mitochondria in mammalian cells. *Mol. Biol. Cell*. 10:4403–4417.

Saxton, W.M., and P.J. Hollenbeck. 2012. The axonal transport of mitochondria. *J. Cell Sci.* 125:2095–2104. http://dx.doi.org/10.1242/jcs.053850

Schneider, C.A., W.S. Rasband, and K.W. Eliceiri. 2012. NIH Image to ImageJ: 25 years of image analysis. *Nat. Methods*. 9:671–675. http://dx.doi.org/10.1038/nmeth.2089

Shpetner, H.S., and R.B. Vallee. 1989. Identification of dynamin, a novel mechanochemical enzyme that mediates interactions between microtubules. *Cell*. 59:421–432. http://dx.doi.org/10.1016/0092-8674(89)90027-5

Song, B.D., M. Leonard, and S.L. Schmid. 2004. Dynamin GTPase domain mutants that differentially affect GTP binding, GTP hydrolysis, and clathrin-mediated endocytosis. *J. Biol. Chem.* 279:40431–40436. http://dx.doi.org/10.1074/jbc.M407007200

Song, Z., H. Chen, M. Fiket, C. Alexander, and D.C. Chan. 2007. OPA1 processing controls mitochondrial fusion and is regulated by mRNA splicing, membrane potential, and Yme1L. *J. Cell Biol.* 178:749–755. http://dx.doi.org/10.1083/jcb.200704110

Strack, S., and J.T. Cribbs. 2012. Allosteric modulation of Drp1 mechanoenzyme assembly and mitochondrial fission by the variable domain. *J. Biol. Chem.* 287:10990–11001. http://dx.doi.org/10.1074/jbc.M112.342105

Szyk, A., A.M. Deaconescu, G. Piszczek, and A. Roll-Mecak. 2011. Tubulin tyrosine ligase structure reveals adaptation of an ancient fold to bind and modify tubulin. *Nat. Struct. Mol. Biol.* 18:1250–1258. http://dx.doi.org/10.1038/nsmb.2148

Taguchi, N., N. Ishihara, A. Jofuku, T. Oka, and K. Mihara. 2007. Mitotic phosphorylation of dynamin-related GTPase Drp1 participates in mitochondrial fission. *J. Biol. Chem.* 282:11521–11529. http://dx.doi.org/10.1074/jbc.M607279200

Tanabe, K., and K. Takei. 2009. Dynamic instability of microtubules requires dynamin 2 and is impaired in a Charcot-Marie-Tooth mutant. *J. Cell Biol.* 185:939–948. http://dx.doi.org/10.1083/jcb.200803153

Thompson, H.M., H. Cao, J. Chen, U. Euteneuer, and M.A. McNiven. 2004. Dynamin 2 binds gamma-tubulin and participates in centrosome cohesion. *Nat. Cell Biol.* 6:335–342. http://dx.doi.org/10.1038/ncb1112

Uo, T., J. Dworzak, C. Kinoshita, D.M. Inman, Y. Kinoshita, P.J. Horner, and R.S. Morrison. 2009. Drp1 levels constitutively regulate mitochondrial dynamics and cell survival in cortical neurons. *Exp. Neurol.* 218:274–285. http://dx.doi.org/10.1016/j.expneurol.2009.05.010

Varadi, A., L.I. Johnson-Cadwell, V. Cirulli, Y. Yoon, V.J. Allan, and G.A. Rutter. 2004. Cytoplasmic dynein regulates the subcellular distribution of mitochondria by controlling the recruitment of the fission factor dynamin-related protein-1. *J. Cell Sci.* 117:4389–4400. http://dx.doi.org/10.1242/jcs.01299

Wakabayashi, J., Z. Zhang, N. Wakabayashi, Y. Tamura, M. Fukaya, T.W. Kensler, M. Iijima, and H. Sesaki. 2009. The dynamin-related GTPase Drp1 is required for embryonic and brain development in mice. *J. Cell Biol.* 186:805–816. http://dx.doi.org/10.1083/jcb.200903065

Walczak, C.E., and S.L. Shaw. 2010. A MAP for bundling microtubules. *Cell*. 142:364–367. http://dx.doi.org/10.1016/j.cell.2010.07.023

Waterham, H.R., J. Koster, C.W. van Roermund, P.A. Mooyer, R.J. Wanders, and J.V. Leonard. 2007. A lethal defect of mitochondrial and peroxisomal fission. *N. Engl. J. Med.* 356:1736–1741. http://dx.doi.org/10.1056/NEJMoa064436

Wilson, T.J., A.M. Slupe, and S. Strack. 2013. Cell signaling and mitochondrial dynamics: Implications for neuronal function and neurodegenerative disease. *Neurobiol. Dis.* 51:13–26. http://dx.doi.org/10.1016/j.nbd.2012.01.009

Xue, J., M.E. Graham, A.E. Novelle, N. Sue, N. Gray, M.A. McNiven, K.J. Smillie, M.A. Cousin, and P.J. Robinson. 2011. Calcineurin selectively docks with the dynamin Ixb splice variant to regulate activity-dependent bulk endocytosis. *J. Biol. Chem.* 286:30295–30303. http://dx.doi.org/10.1074/jbc.M111.273110

Yoon, Y., K.R. Pitts, S. Dahan, and M.A. McNiven. 1998. A novel dynamin-like protein associates with cytoplasmic vesicles and tubules of the endoplasmic reticulum in mammalian cells. *J. Cell Biol.* 140:779–793. http://dx.doi.org/10.1083/jcb.140.4.779

Youle, R.J., and A.M. van der Bliek. 2012. Mitochondrial fission, fusion, and stress. *Science*. 337:1062–1065. http://dx.doi.org/10.1126/science.1219855